1963

Positron mean lives in metals

John Landon Rodda II
Iowa State University

POSITRON MEAN LIVES IN METALS

by

John Landon Rodda II

A Dissertation Submitted to the
Graduate Faculty in Partial Fulfillment of
The Requirements for the Degree of
DOCTOR OF PHILOSOPHY

Major Subject: Physics

Approved:

Signature was redacted for privacy.

In Charge of Major Work

Signature was redacted for privacy.

Head of Major Department

Signature was redacted for privacy.

Dean of Graduate College

Iowa State University
Of Science and Technology
Ames, Iowa

1963

TABLE OF CONTENTS

I. INTRODUCTION

If a positron is injected into a metallic sample with an energy of a few hundred kilovolts it will be able to penetrate to the interior of the sample. There it will be thermalized in about 3×10^{-12} sec (1) via collisions with conduction electrons, and it will become part of the electronic system. Some time later the positron will annihilate with an electron, producing (usually) two 0.511 Mev annihilation gamma rays. These relatively high energy gamma rays can then bring information about the annihilation process out of the sample with negligible attenuation or scattering.

The positron mean life characteristic of a particular metal often depends only on the product of the positron wave function times the wave function of the electron with which it annihilates (2, p. 308). Thus the measurement of the positron mean life in a metal should provide some information on the electronic structure of the metal. The positron can, of course, strongly affect the electronic configuration of the metal, and this must be taken into account when interpreting the results of these measurements.

The first extensive measurements of positron mean lives in metals were made by Bell and Graham (3, 4), and since then numerous measurements have been made by these and other investigators. These measurements indicate that the

positron mean life in a metal is on the order of 2×10^{-10} sec, and for most of the metals thus far investigated it is independent of the metal chosen within about $\pm$ 25%. Thus it is evident that in order to detect meaningful variations in positron lifetimes between various metals, the lifetimes should be measured with a relative uncertainty approaching one percent. This then implies that the positron lifetimes in various metals must be made with a relative time uncertainty not much larger than $\pm 2 \times 10^{-12}$ sec (which is the time it takes light to travel 0.6 mm in a vacuum).

The presently existing theories are not sufficiently accurate to make quantitative predictions of positron lifetimes in metals. The present investigation was thus undertaken in order to make some of the more accurate measurements which are necessary in order to point the way for refinements in the theory. The particular measurements reported in this dissertation include the absolute positron mean life in aluminum and the relative (to aluminum) positron mean lives in all the stable metals in Group III B of the periodic table and in samples of sodium tungsten bronze (Na_xWO_3) for a number of values of x. The relative lifetimes are believed to be correct to within $\pm 3 \times 10^{-12}$ sec.

II. THEORETICAL DISCUSSION

A. The Annihilation Process

In 1950 DeBenedetti *et al.* (5, pp. 210-212) calculated that the time for positron thermalization in gold by the excitation of lattice vibrations is 3×10^{-10} sec. Garwin (6) pointed out, however, that a positron which is no longer energetic enough to cause interband transitions will lose energy primarily by collisions with conduction electrons. He estimated the thermalization time in metals to be about 10^{-13} sec (including free electron screening). Detailed calculations by Lee-Whiting (1) yield a thermalization time in metals of 3.2×10^{-12} sec. Since the positron mean life in metals is about 2×10^{-10} sec, we can thus conclude that the positrons are completely thermalized prior to annihilation.

In order to conserve energy and momentum when a positron and an electron annihilate, at least two photons must be emitted (unless there is a sufficiently strong external field present to absorb the momentum, or unless a third particle participates in the interaction). Since the positron and electron have energies much less than mc^2, the two quanta have energies of about 0.511 Mev each and are emitted in nearly opposite directions in the laboratory system.

Because of the small relative energy of the pair

before annihilation, only for S states will the positron and electron wave functions overlap appreciably. Two-photon annihilation, however, is completely forbidden for all J = 1 states (7, p. 242), and so it can not occur via $^3S_1$ states. Two-quantum annihilation thus occurs predominately in $^1S_0$ states. From a classical point of view this means that the two particles collide head on and with opposite spins.

When two-quantum annihilation is completely forbidden, three-quantum annihilation will occur. Thus a positron-electron pair can annihilate via the $^3S_1$ state with the emission of three quanta. The ratio of the three-quantum to two-quantum rate has been calculated by Ore and Powell (8) who find $R_{3q}/R_{2q} = (4/9\pi)(\pi^2-9)(e^2/\hbar c) \cong 1/1115$. For randomly distributed electron spins the triplet configuration is three times as likely as the singlet configuration. Thus the corresponding cross section ratio is $\sigma_{3q}/\sigma_{2q} = 1/372$, and hence three-quantum annihilation is a very small effect. If a bound system such as positronium is formed, however, then the electron spins become oriented with respect to the positron spins, and the three-quantum process becomes more important (because of the decay of ortho-positronium).

B. Other Types of Annihilation Experiments

From the above discussion it is evident that there are other positron annihilation experiments that one can do besides

measuring the lifetime for two-quantum annihilation. Review articles which discuss the various types of positron annihilation experiments are available (2, 9, 10, 11, 12, 13, 14), so only two of the most important experiments will be discussed briefly here.

1. Three-photon rate

One can, for example, measure the ratio of the number of two-quantum events to the number of three-quantum events, and if no bound positron states are formed this ratio should be 372. Rough measurements by Rich (15) confirmed this ratio within a factor of two for aluminum, and the more accurate measurements of Basson (16) yielded $\sigma_{2q}/\sigma_{3q} = 402 \pm 50$. Graham and Stewart (17), however, have found that the three-quantum annihilation rate in fuzed quartz, polystyrene, and teflon is two or three times that in aluminum, and thus conclude that positronium is formed in these substances. Two-quantum annihilation lifetime measurements by Bell and Graham (4) also show that there are two distinct positron lifetimes in these substances, and the longer lifetime, τ_2, is believed to represent the conversion rate between triplet and singlet positronium. Thus the three-photon rate does not give independent information, since it is proportional to the product of the fraction of positrons forming positronium times the long lifetime, and hence can also be determined from the

lifetime measurements. All subsequent discussion will thus refer only to the two-photon mode of annihilation.

2. Angular correlation of photons in two-quantum annihilation

The two photons are not always emitted in exactly opposite directions because they must carry off the momentum of the electron which is annihilated. Measurement of the angular correlation between the two photons thus should give information about the momentum distribution of the annihilating electrons. This type of experiment was first done by DeBenedetti *et al.* (5) using gold. They found that the mean momentum of the annihilating pairs is 1.2 mc/137, in rough agreement with a theoretical lower limit of 0.8 mc/137. These data indicated that the positrons are indeed quite well thermalized and that they annihilate primarily with the valence electrons.

More extensive measurements were later made by Green and Stewart (18), Stewart (19, 20), Lang *et al.* (21), and Lang and DeBenedetti (22). The measured distributions for metals fall into two general classes: those consisting of a central inverted parabola plus a tail at larger angles (e.g. aluminum), and those better represented by a Gaussian distribution (e.g. copper). Berko and Plaskett (23) have shown that the central portions of both the aluminum and the copper distributions can be attributed to valence electron annihilation, while the small tail on the aluminum and the large tail

on the copper can be attributed to core annihilation with L shell and M shell electrons, respectively. Thus these experiments allow one to estimate the percentage of core annihilation which takes place.

Metals which exhibit the parabolic type of distribution have a fairly sharp cutoff in the distribution at an angle given by $\hbar k'/mc$, where k' is the wave number at the Fermi surface as calculated from the free electron theory. Thus angular correlation experiments with oriented single crystals should allow one to study the anisotropy of the Fermi surface in metals of this type. Such experiments have recently been done by Stewart et al. (24) and Berko (25), and indicate a marked anisotropy of the Fermi surface in beryllium. Berko's (25) results for magnesium, and Berko and Plaskett's (23) results for aluminum and copper, however, indicate a nearly spherical Fermi surface for these metals.

Angular correlation measurements on teflon by Stewart (19) and fuzed quartz by Page et al. (26) display sharp peaks in the angular distributions at the zero angle positions. This is thought to be due to the annihilation of low energy positronium, and is associated with the increased three-photon annihilation rate found for these materials by Graham and Stewart (17) and the long lived, τ_2, component found by Bell and Graham (4).

C. Theoretical Predictions of Annihilation Rates

1. Free electron theory

Since the positrons are thermalized prior to annihilation, a first approach to the problem is to use the Dirac cross section for the annihilation of a slow free positron by a slow electron (27):

$$\sigma_a = \frac{\pi r_o^2 c}{v} \tag{1}$$

where r_o is the classical electron radius (e^2/mc^2) and v is the relative velocity of the electron and the positron. (It is interesting to note that this formula was derived in 1930 before the positron had been discovered.) Thus, assuming that only the conduction electrons take part in the annihilation process, the annihilation rate is given by

$$\lambda = nv\sigma_a = (\pi r_o^2 c)n \tag{2}$$

where n is the density of conduction electrons.

Often the electron density is specified in terms of r_s, the radius of a sphere containing one conduction electron (the so-called unit conduction electron sphere). Thus the volume per electron is

$$\frac{1}{n} = \frac{4}{3}\pi(a_o r_s)^3 \tag{3}$$

where the Bohr radius, a_o, is included in the definition so that r_s will be dimensionless. Now $n = (N_o z\rho/A)\ cm^{-3}$, where N_o is Avogadro's number, and z, ρ, and A are the metallic valence, density, and atomic weight, respectively. Thus Equation 3 yields

$$r_s = 1.384\ (A/\rho z)^{1/3} \tag{4}$$

which allows the direct computation of r_s. Substituting Equation 3 into Equation 2 gives

$$\lambda = 12\ r_s^{-3} \times 10^9\ sec^{-1} \tag{5}$$

as an alternative form for Equation 2.

Equation 2 (or Equation 5) indicates that the annihilation rate is proportional to the density of conduction electrons. Each metal, then, is distinguished only by a certain value of electron density, and thus this formula is the Sommerfeld free electron approximation. Even where other considerations lead one to expect that the Sommerfeld theory might apply, however, this formula gives annihilation rates that are much smaller than those found experimentally. As a matter of fact, most metals have the same positron lifetime within about 25% (28, p. 663), while it is obvious that lifetimes calculated from the above formula will vary widely from metal to metal. For example, $r_s = 1.62$ for tungsten and $r_s = 3.01$ for gold. Thus Equation 5 predicts $\tau_{AU}/\tau_W = \lambda_W/\lambda_{AU} =$

$(3.01/1.62)^3 = 6.4$, while it is found experimentally (29, 30) that $\tau_{AU}/\tau_W = 1 \pm .25$.

Obviously the free electron treatment is not satisfactory. One reason is that it uses the average electron density in the metal, and the actual electron density at the position of the positron will be larger because of the Coulomb attraction (neglected by the Dirac formula) exerted on the electrons by the positron. This polarization of the electron gas must, of course, be reduced to the extent that the repulsive interactions between the electrons screen the positron from more distant electrons. A complete treatment should also include the effects of the Pauli exclusion principle and the Heisenberg uncertainty principle upon the polarization of the electron gas.

2. Radiation theory

By means of second order perturbation theory De-Benedetti *et al.* (5) and Ferrell (2) have derived the following formula for the two-quantum annihilation rate for the case in which the electron-positron wave function is separable:

$$\lambda = \pi r_o^2 c \int |\psi_+(\bar{r})\psi_-(\bar{r})|^2 d\bar{r} \quad . \qquad (6)$$

This equation states that the annihilation rate is proportional to the electron density, integrated over the position of the positron.

A simple application of Equation 6 is to the ground state of positronium. This bound system is very similar to the hydrogen atom except that its reduced mass is approximately half that of the hydrogen atom. Thus the positronium wave functions will be just those of the hydrogen atom (31, pp. 80-86) with the Bohr radius, a_o, replaced by $2a_o$. Thus

$$\lambda = \pi r_o^2 c |\psi_{100}(0)|^2$$

$$= \pi r_o^2 c \left| \frac{1}{\sqrt{4\pi}} (2a_o)^{-3/2} 2e^{-0/2a_o} \right|^2 \qquad (7)$$

$$= 2.0 \times 10^9 \text{ sec}^{-1}$$

or

$$\tau = \frac{1}{\lambda} = 5.0 \times 10^{-10} \text{ sec} \quad . \qquad (8)$$

This, however, is a spin averaged lifetime. Since two-quantum annihilation is allowed only for the singlet state, the singlet lifetime will be one-quarter of this value, or

$$\tau_s = 1.25 \times 10^{-10} \text{ sec} \quad . \qquad (9)$$

It is interesting to note that no lifetimes have ever been measured that are shorter than this value.

As was noted in Section A, the two-photon annihilation rate is 1115 times the three-photon rate. Thus the lifetime of the triplet state (against three-quantum annihilation) is

$$\tau_t = 1115 \times \tau_s = 1.4 \times 10^{-7} \text{ sec} . \qquad (10)$$

It should be noted here that even in solids in which positronium is formed, the longest observed lifetime is a factor of 50 shorter than this. This is due to rapid triplet to singlet conversion (through spin exchange) and to annihilation of the bound positron with an external electron.

3. Ferrell enhancement

A consistent quantum mechanical treatment will automatically include the exclusion and uncertainty principles. The Coulomb interaction (which enhances the electron density at the position of the positron), however, makes an exact treatment impossible, and it is too strong to be treated as a perturbation. Ferrell (2) attacked the problem by separating out the long-range, collective response of the electrons to the positron in the manner of Bohm and Pines (32). He then treated the remaining weaker, short-range (screened), electron-positron interaction as a perturbation in order to calculate the first order correction to the electron-positron wavefunction. The final result is a considerable enhancement of the Sommerfeld annihilation rate (Equation 5) and a reduced dependence of λ upon r_s. Unfortunately, however, the dependence is still much too strong to fit the experimental data.

4. Kahana theory

Kahana (33) claims his calculations indicate that the screened electron-positron Coulomb force is too strong to be treated as a perturbation. He obtains an approximate solution to the appropriate Bethe-Goldstone equation (34) embodying the screened Coulomb positron-electron interaction and the Pauli exclusion principle. Because of the lack of a digital computer he computed the annihilation rate for only three values of r_s. The results seem to give about the same variation of λ with r_s as is found experimentally, but the predicted annihilation rates are about a factor of two larger than those found experimentally. Whether this is due to the approximations made or to the model is not yet clear.

In summary we note, following Wallace (14), that all of the above theories neglect the lattice potential, and quantitative agreement between theory and experiment may not come until it is possible to replace free-particle states in the calculations with Bloch states.

III. EXPERIMENTAL METHOD

A. Positron Source

In order to determine the positron lifetime in a metal, a Na^{22} source is sandwiched between two pieces (thick enough to stop all of the positrons) of the metal under investigation. The decay scheme of Na^{22} is shown in Figure 1. The decay (with a half-life of 2.6 years) is almost entirely to the 1.28 Mev excited state of Ne^{22}, either by electron capture (10.2%) or by positron emission (89.8%) with an end point energy of 0.54 Mev. Since the lifetime (3.3×10^{-12}sec) of this excited state is short compared with the positron mean life in a metal ($\sim 2 \times 10^{-10}$sec), the positron and the 1.28 Mev de-excitation gamma ray can be considered to be emitted simultaneously. The problem of measuring the positron mean life in a metal is thus reduced to measuring the mean time between the detection of the 1.28 Mev gamma ray, which the Na^{22} emits simultaneously with a positron, and the detection of one of the 0.511 Mev gamma rays produced when the positron later annihilates in the metal sample.

B. Basic Circuits

1. General description

A simplified block diagram of the electronics is shown in Figure 2. The detectors are 1-1/2 x 1 in. Naton 136

Figure 1. Decay scheme of Na^{22}. Because the lifetime of the 1.28 Mev state is very short compared to the positron mean life in a metal, the positron and the 1.28 Mev gamma ray can be considered to be emitted simultaneously.

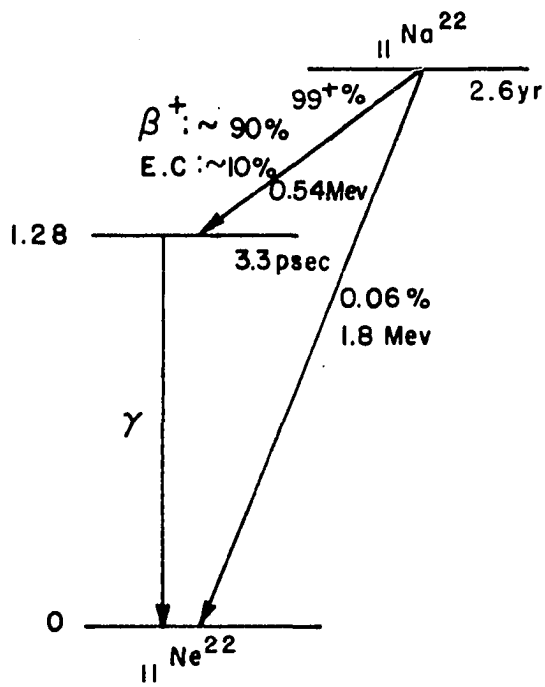
11 Na22
2.6yr
99+%
β+: ~ 90%
E.C :~10%
0.54Mev
1.28
3.3psec
0.06 %
1.8 Mev
γ
0
11 Ne22

Figure 2. Simplified block diagram of the electronics

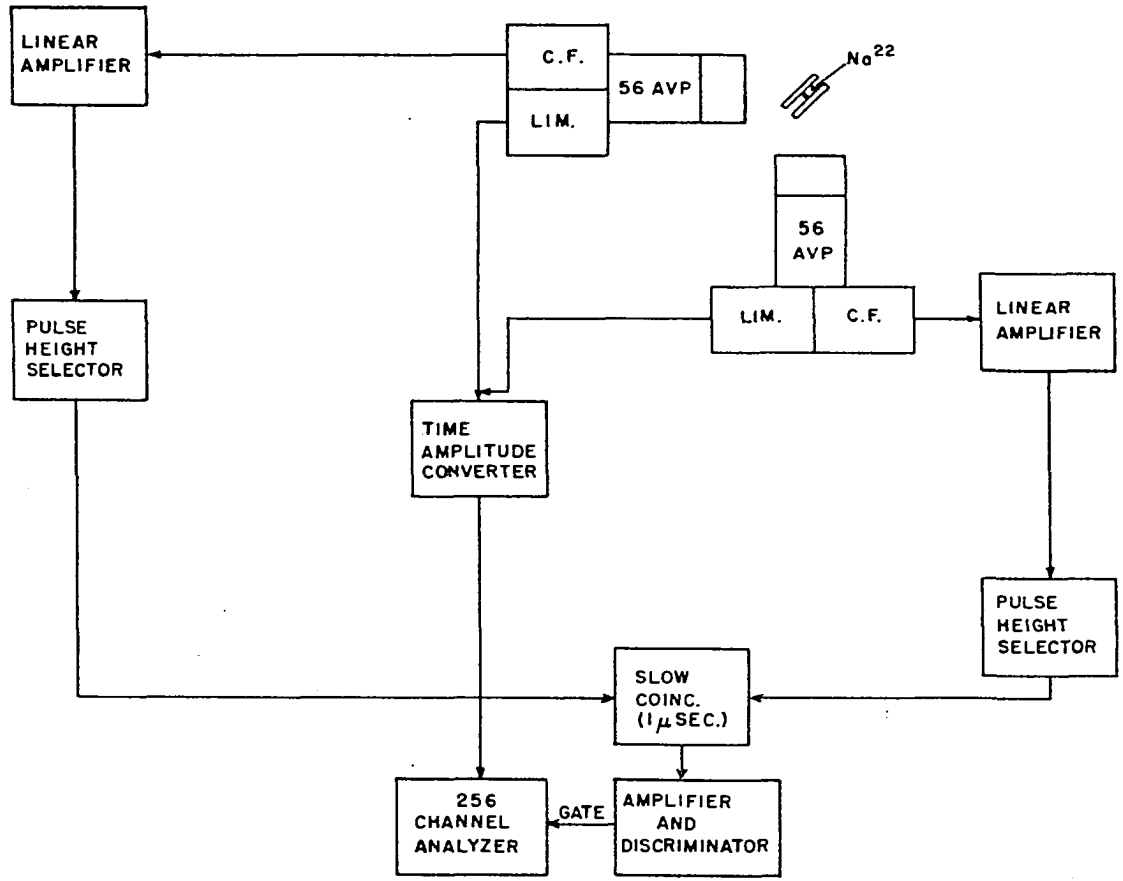
LINEAR AMPLIFIER
C.F.
LIM.
56 AVP
Na^{22}
56 AVP
LIM.
C.F.
LINEAR AMPLIFIER
PULSE HEIGHT SELECTOR
TIME AMPLITUDE CONVERTER
PULSE HEIGHT SELECTOR
SLOW COINC. (1μSEC.)
256 CHANNEL ANALYZER
GATE
AMPLIFIER AND DISCRIMINATOR

plastic scintillators (available from Nash and Thompson Limited, Hook Rise South, Tolworth, Surbiton, Surrey, England) coupled to Amperex 56 AVP photomultiplier tubes.

When a positron is emitted from the Na^{22} source the simultaneously emitted 1.28 Mev gamma ray is detected in the upper detector. The resulting pulse at the photomultiplier anode cuts off a high transconductance pentode limiter, producing a fast-rising, flat-topped output pulse to a time amplitude converter (TAC). Sometime later the positron will annihilate in the metallic sample, producing two gamma rays. One of these gamma rays is detected in the lower detector, and again a limited pulse is produced.

The two limited pulses are fed into the TAC, which produces an output pulse whose height is proportional to the time delay between the two input pulses. This output pulse is then fed to an Argonne type multichannel analyzer (Radiation Counter Laboratories Mark 20, Model 2603) which separates the incoming pulses according to their height. Thus the output data from the analyzer is the distribution of events corresponding to various time delays between the 1.28 Mev and the 0.511 Mev gamma rays, i.e. the delayed time spectrum for positron annihilation in the particular metal being studied.

The only events to be analyzed are those for which the 1.28 Mev gamma ray enters the upper detector and one of the 0.511 Mev gamma rays enters the lower detector, and this

restriction requires the use of auxiliary equipment. A cathode follower at the eighth dynode of each phototube drives a linear amplifier (Cosmic Radiation Laboratories Model 101) and a Fairstein and Porter type pulse height selector (35, 36) which has been modified to trigger on the leading edge of the input pulse instead of the trailing edge. The pulse height selector corresponding to the upper detector is set with an integral discriminator on the upper one-third of the Compton distribution from the 1.28 Mev gamma rays, and the selector corresponding to the lower detector is set with a window on the upper one-third of the Compton distribution from the annihilation gamma rays. The two pulse height selectors drive a slow coincidence circuit whose output is fed to a combination amplifier and discriminator (Atomic Model 204C). The discriminator, having been slightly modified to produce the proper type of pulse, is then used to gate the analyzer. Thus the analyzer will accept an input pulse from the TAC only for those events in which the 1.28 Mev gamma ray enters the upper detector and one of the annihilation gamma rays enters the lower detector.

2. Photomultiplier, cathode follower, and limiter circuits

The photomultiplier, cathode follower, and limiter circuits are shown in Figure 3. The high voltage supplies for the photomultiplier tubes are a Smith-Florence Model 122 and a New Jersey Electronics Model S-325, while the B^+ supply is a

Figure 3. Photomultiplier, cathode follower, and limiter circuits. The limiter is a very slight modification of the circuit described by Simms (37).

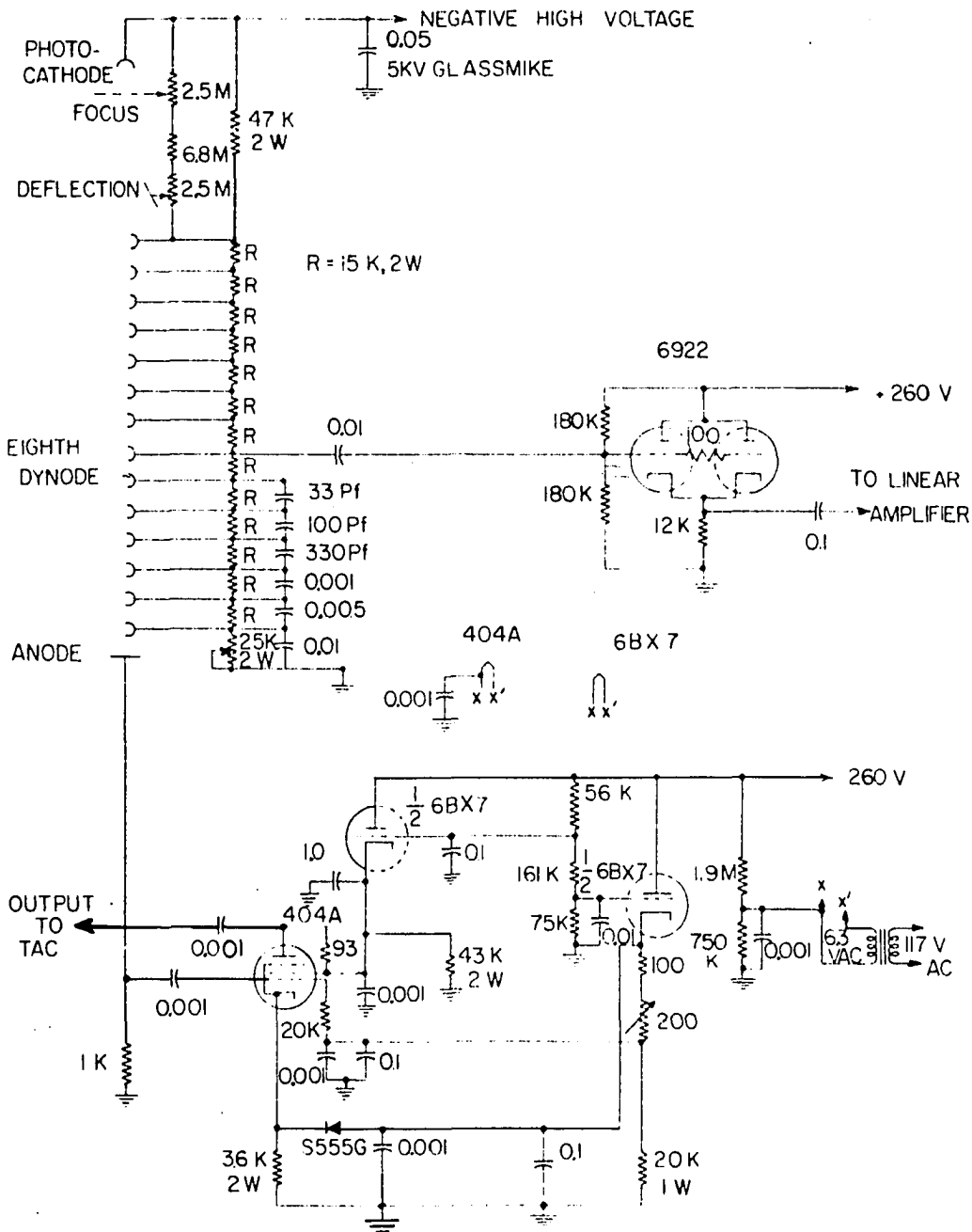
NEGATIVE HIGH VOLTAGE
0.05
5KV GLASSMIKE
PHOTO-CATHODE
FOCUS
2.5M
47 K 2 W
6.8M
DEFLECTION
2.5M
R = 15 K, 2W
EIGHTH DYNODE
ANODE
0.01
33 Pf
100 Pf
330Pf
0.001
0.005
25K 2W
0.01
6922
+260 V
180K
180K
100
12K
0.1
TO LINEAR AMPLIFIER
404A
6BX7
0.001
260 V
56 K
1/2 6BX7
1.0
0.01
161 K
1/2 6BX7
1.9M
OUTPUT TO TAC
404A
0.001
93
43 K 2 W
0.001
75K
0.01
100
750 K
0.001
6.3 VAC
117 V AC
0.001
20K
0.01
0.001
200
1 K
S555G
0.001
0.1
36 K 2W
20K 1W

Kepco Model KR4M. The phototube high voltage is set at about 1770 volts, because higher voltages produce ringing on the limiter output pulses (viewed with a Tektronix Type N sampling unit), and thus cause the time calibration to be nonlinear. The focus, deflection, and last dynode voltages are set to optimize the shape of the limiter output pulse.

The 404A limiter is a very slightly modified version of that described by Simms (37, pp. 895-896). When a photomultiplier anode pulse cuts off the 404A, a rast rising (~2 nanoseconds), flat-topped, positive pulse is produced at the plate of the 404A. This pulse is coupled to the TAC with Rg-62/U cable which is terminated by the 93 ohm plate resistor of the limiter. The S555G diode allows the tube current to return rapidly to the quiescent value, and the 6BX7 tube helps to maintain the constant quiescent tube current required if the output pulses are to have a constant amplitude.

The 6922 cathode follower is capacity coupled to the eighth dynode of the phototube. This circuit is quite straightforward and requires no further discussion.

3. Slow coincidence circuit

The slow coincidence circuit shown in Figure 4 is basically a Garwin circuit (38) with the triodes replaced by diodes in the manner of Madey (39, pp. 973-974). A negative pulse from either pulse height selector triggers one of two transistorized blocking oscillators. These oscillators produce

Figure 4. Slow coincidence circuit. The output of this circuit gates the multichannel analyzer on when a 1.28 Mev gamma ray and an annihilation gamma ray interact simultaneously (within 1 μsec) in their respective detectors. The anti-coincidence input is used to reject events which correspond to the roles of the two gamma rays being reversed.

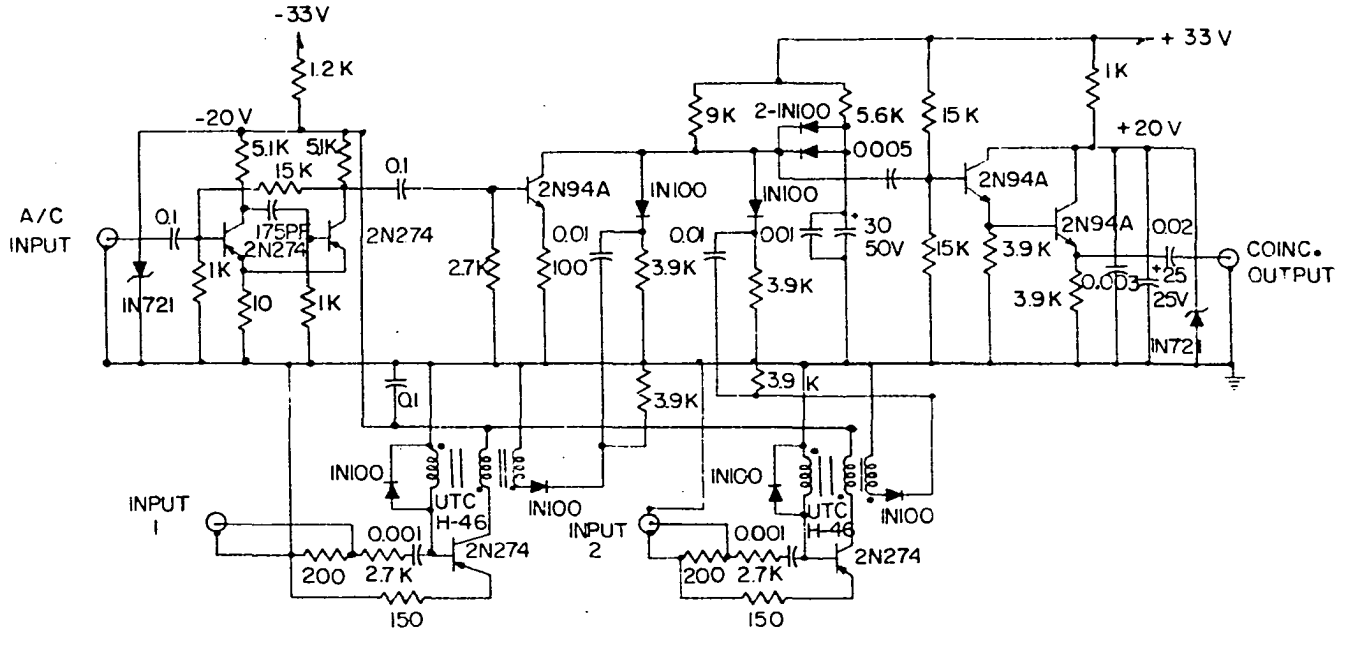
-33V
1.2K
-20V
5.1K
5.1K
15K
0.1
A/C
INPUT
0.1
175PF
2N274
2N274
1K
IN721
10
1K
2.7K
2N94A
0.01
100
IN100
3.9K
9K
2-IN100
5.6K
0005
IN100
0.01
001
30
50V
3.9K
15K
15K
1K
+33V
+20V
2N94A
3.9K
2N94A
0.002
0.003
+25
25V
IN721
COINC.
OUTPUT
0.1
3.9K
3.9K
IN100
UTC
H-46
2N274
IN100
INPUT
1
0.001
200
2.7K
150
IN100
INPUT
2
0.001
200
2.7K
150
IN100
UTC
H-46
2N274
IN100

+10 volt, 0.5 μsec pulses which cut off the 1N100 coincidence diodes. If both diodes are cut off at the same time, a +4 volt coincidence pulse is produced. When only one diode is cut off a much smaller (~0.5 volt) pulse is produced. A two stage emitter follower is used to couple the output to the gate amplifier and discriminator, and the discriminator is set so as to reject all singles pulses.

The 2N94A transistor to the left of the coincidence diodes furnishes an anti-coincidence input to the circuit. If a positive pulse triggers the 2N274 single-shot multivibrator, it will produce a +10 volt, 3 μsec pulse which will turn on the (normally off) anti-coincidence transistor. Thus any coincidence occuring during this 3 μsec period will produce no output, because the current normally carried by the coincidence diodes will be shunted to the 2N94A transistor. This anti-coincidence input is used to eliminate a certain type of background, and will be discussed in more detail in Section E of this chapter.

4. Time-amplitude converter

The TAC is a circuit which accepts two rectangular input pulses and produces an output pulse proportional to the time delay between the two input pulses. This is accomplished by adding the rectangular pulses across a non-linear element which is back-biased above the level of a single pulse. The output from the non-linear element is integrated to give a

pulse proportional to the area of overlap of the input pulses. Thus, if the input pulses have a constant amplitude, this area is proportional to the delay between the input pulses.

The TAC used for the present work is a simple modification of the biased diode circuit described by Bell *et al.* (40). The circuit requires no auxiliary amplifiers and the output is of the correct polarity, amplitude, and shape for direct application to most multichannel analyzers.

An elementary form of the TAC is shown in Figure 5. Individual pulses from the limiters are delay-line clipped in standard fashion to about 12 nanoseconds at the base of a fast silicon NPN transistor. Pulses which overlap in time create a potential (about 1 volt) sufficient to override the base-emitter cut-off bias of the transistor, and carriers are injected towards the collector. The capacitor C_i at the collector acts as an integrating capacitor, and it is charged by the injected carriers to a potential proportional to the time duration of the pulse overlap. The time constant $R_L C_i$ is very long with respect to the charge collection or rise time, and since the transistor is cut off following the pulse rise, the decay time is determined by $R_L C_i$.

Figure 6 is the circuit as it is actually used, the input cables and delay-line clipper being omitted from the figure for simplicity. The emitter of T1 is now biased through an emitter follower, T2, of the same type. This is done to

Figure 5. Simplified version of the time-amplitude converter. This circuit produces an output pulse whose height is proportional to the time delay between the two input pulses.

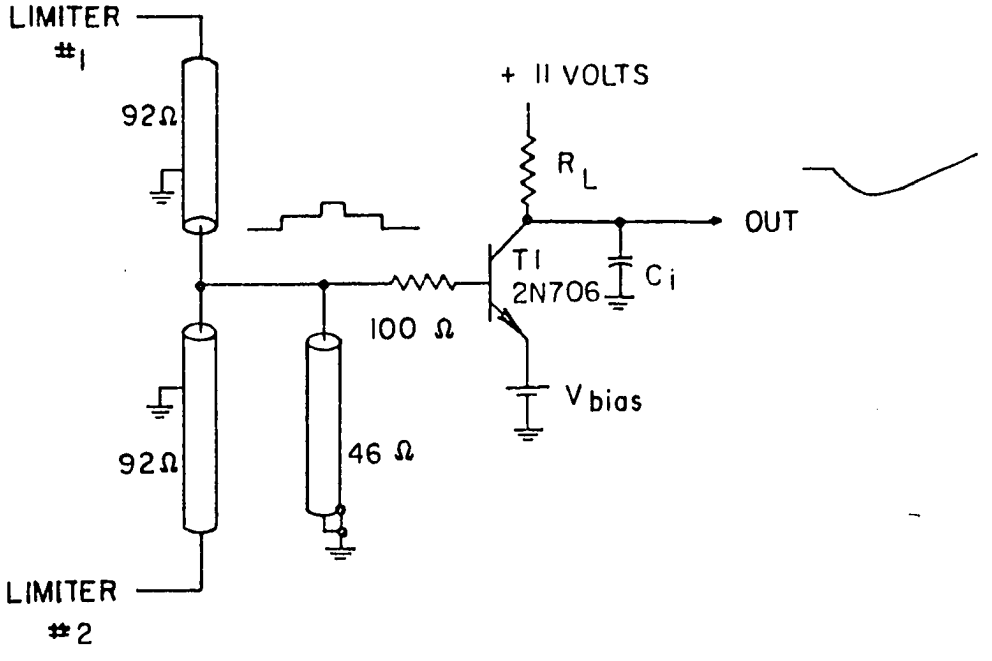
LIMITER
#1
92Ω
+ 11 VOLTS
R_L
OUT
T1
2N706
C_i
100 Ω
V_{bias}
92Ω
46 Ω
LIMITER
#2

Figure 6. The time-amplitude converter. This circuit has better integrating qualities than that shown in Figure 5. It is also temperature compensated, and it has an emitter follower output stage.

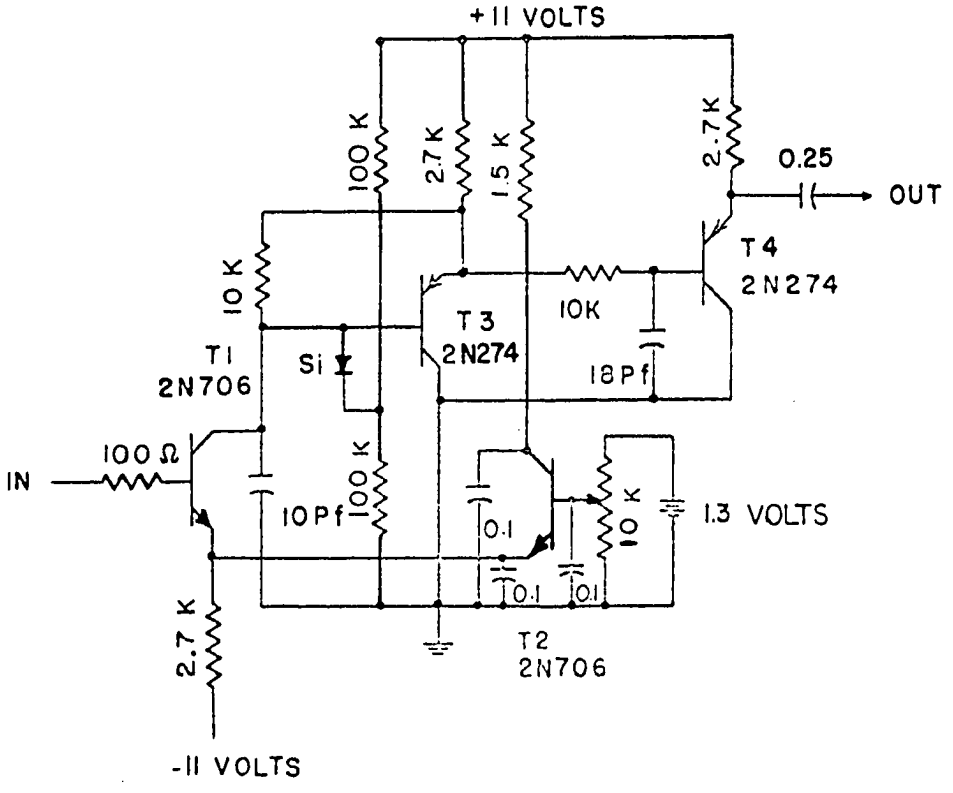
+11 VOLTS
100 K
2.7 K
1.5 K
2.7K
0.25
OUT
T4
2N274
10 K
T3
2N274
10K
T1
2N706
Si
18Pf
100 Ω
IN
100 K
10Pf
0.1
10 K
1.3 VOLTS
0.1
0.1
2.7 K
T2
2N706
-11 VOLTS

reduce the temperature sensitivity of the bias level.

The collector circuit of T1 consists of a bootstrap emitter follower circuit. This causes an increase in the effective load resistance to T1, resulting in a slight improvement of the integrating qualities and a relatively long pulse decay time. The rise time at the emitter of T3 is still much faster than that required by conventional pulse height analyzers, so the pulses are coupled through a lag network to the base of T4, which is the output emitter follower.

Since T1 is normally cut off, a small current is delivered to the base of T3 through a silicon switching diode. This established a reasonable operating point for the emitter followers and a stable pulse base line.

The output of the TAC decreases by about 0.55×10^{-10} sec/^{o}C. between 35 and 40^{o}C. To minimize this effect, the TAC is placed in an enclosed, insulated chassis and maintained at 37.0 ± 0.2 ^{o}C. with a transistorized thermostatic control (41). Heat is supplied by several 6 watt pilot lamps, and a uniform temperature is maintained by circulating air with a small blower.

C. Time Resolution

When the equipment described above is used to obtain the prompt time spectrum from two simultaneous gamma rays

(e.g. the gamma ray cascade in Co^{60}) it is found that all of the counts are not confined to a single channel on the analyzer (i.e. to a single delay). The counts are actually spread out over a number of channels in a distribution that is nearly parabolic when plotted on a semi-logarithmic scale. This finite time resolution is usually specified by 2τ, the full width at half height on the time spectrum, and for the prompt Co^{60} spectrum shown in Figure 7, $2\tau = 5.70 \times 10^{-10}$ sec. The two main factors limiting the resolution will be discussed below.

1. Phosphor decay time

When a gamma ray Compton scatters in a scintillator, the scattered electron produces a light flash which decays approximately exponentially (for organic scintillators) (42) with some mean life τ_p. This light flash produces photoelectrons at the cathode of the phototube, and they in turn are multiplied in the phototube to produce an anode pulse. It takes a time t to produce the N photoelectrons required to give an anode voltage V large enough to cut off the limiter tube. The time t, however, is subject to statistical fluctuations, and these fluctuations produce an imperfect time resolution.

Post and Schiff (43) have shown that the average time $\bar{t}$ to produce N photoelectrons is

Figure 7. Time spectrum of positron annihilation in aluminum. The prompt curve is a measurement of the Co^{60} gamma rays using the same settings as for the positron measurements. The centroid shift is $(2.24 \pm 0.05) \times 10^{-10}$ sec, using a time calibration of 6.37×10^{-11} sec/channel.

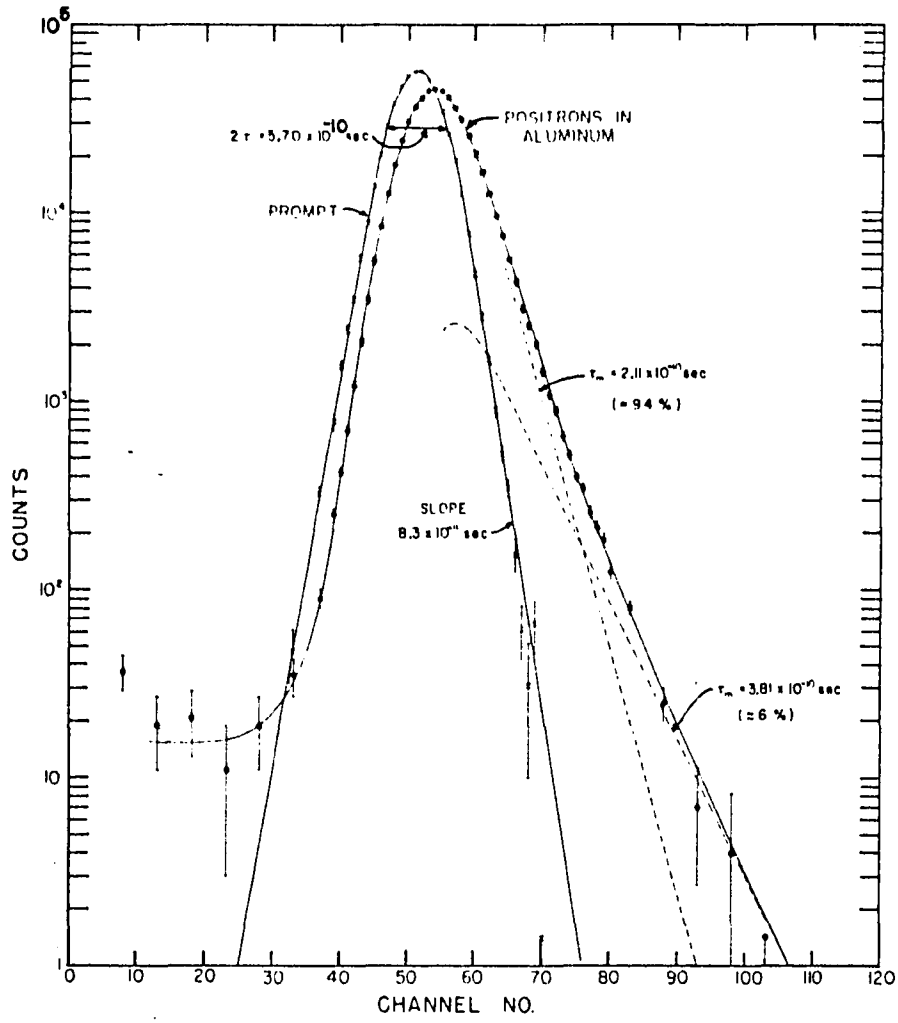
COUNTS
CHANNEL NO.
POSITRONS IN ALUMINUM
PROMPT
SLOPE
(≈ 94 %)
(≈ 6 %)

$$\bar{t} \cong \frac{N\tau_p}{R}\left(1 + \frac{N+1}{2R}\right) \tag{11}$$

where R is the average total number of primary photoelectrons. They have also shown that the rms deviation from this time is

$$\sqrt{v} = \sqrt{\langle t^2\rangle_{av.} - \bar{t}^2} \cong \frac{\bar{t}}{\sqrt{N}}\left(1 + \frac{N+1}{R}\right)^{1/2} \tag{12}$$

Equations 11 and 12 indicate that in order to keep the deviation to a minimum, τ_p/R must be kept as small as possible.

In order to produce the V = 3 volts needed to cut off the limiter, a charge Q must be collected at the anode of the phototube. If the gain of the phototube is A, then this charge is given by

$$Q = CV = NeA$$

or

$$N = \frac{CV}{eA} \tag{13}$$

where C is the total capacitance from the anode to ground, and is on the order of 25 picofarads. This includes the anode capacitance, the limiter grid capacitance, and the wiring capacitance. At 1770 volts the photomultiplier gain is about 2.5×10^7. Thus Equation 13 yields $N \sim 19$ photoelectrons.

The quantities τ_p and R, which must be known before

Equations 11 and 12 can be solved, are to be chosen so as to minimize τ_p/R. Now NaI (Tℓ) is the most efficient phosphor known, and hence it will have the largest value of R. The decay constant, τ_p, for NaI (Tℓ), however, is 2.5×10^{-7} sec (44, p. 57), and it is similarly long for all of the reasonably efficient inorganic phosphors. Certain organic phosphors, on the other hand, have decay constants 10 to 100 times smaller than NaI (Tℓ), and yet are up to 25 or 50% as efficient. Anthracene, for example, has $\tau_p = 30 \times 10^{-9}$ sec (44, p. 90) and is half as efficient (44, p. 52) as NaI (Tℓ), while stilbene has $\tau_p = 8 \times 10^{-9}$ sec and is about one-fourth as efficient as NaI (Tℓ). The Naton 136 plastic scintillator used in present investigation is even better, being about 30% as efficient as NaI (Tℓ), and having a decay time that is probably about 3×10^{-9} sec.

Bell et al. (40, p. 36) estimate that a Compton electron of energy E interacting in an anthracene phosphor will produce $R \sim E/3$ (E in kev) photoelectrons in a 1P21 phototube. Naton 136 is only 60% as efficient as anthracene, but the luminous sensitivity of the 56 AVP phototube used in the present investigation is perhaps 60% larger than for the 1P21. Thus $R \sim E/3$ may not be an unreasonable estimate to use for the present case. The maximum energy that an annihilation gamma ray can transfer to an electron in a Compton collision is 0.340 Mev, so the average electron energy in the

upper one-third of the distribution is probably $\sim$ 0.260 Mev. Thus R $\sim$ 85 photoelectrons is probably a reasonable estimate.

Substituting N = 19, $\tau_p = 3 \times 10^{-9}$ sec, and R = 85 into Equation 11 yields $\bar{t}_{0.51} \sim 7.5 \times 10^{-10}$ sec. Equation 12 then gives $(\sqrt{v})_{0.51} \sim 1.9 \times 10^{-10}$ sec for the rms deviation. A similar calculation for the upper one-third of the Compton distribution of the 1.28 Mev gamma rays yields $(\sqrt{v})_{1.28} \sim 1.6 \times 10^{-10}$ sec. Thus the resolution is limited by the scintillator characteristics to

$$2\tau_s \sim \sqrt{(1.9)^2 + (1.6)^2} \times 10^{-10} = 2.5 \times 10^{-10} \text{ sec} . \quad (14)$$

2. Phototube transit-time spread

If the photomultiplier tube had perfect acceleration characteristics, then the overall time resolution for prompt gamma rays would be roughly that given by Equation 14. The time for a photoelectron to travel from the photocathode to the first dynode, however, is not a constant, but varies with its initial position and energy. There is also some transit-time spread between the dynodes of the tube. The spread between the photocathode and the first dynode, however, is by far the most important, because of the large size of the cathode compared to the dynodes, and because of the variation in energy of the electrons leaving the cathode.

By carefully designing the phototube, the transit-time spread can be made quite small. The 56 AVP tube used in the

present investigation has a curved photocathode and a complicated focusing and deflecting electrode structure which together limit the transit-time spread to about 3×10^{-10} sec (for a 1-1/2 in. diameter phosphor and a high voltage of 2000 volts). This is a considerably smaller spread than that which is inherent in the other fourteen stage tubes currently available. The transit-time spreads in the 6810A and 7264, for example, are (again at 2000 volts with a 1-1/2 in. diameter phosphor) 3×10^{-9} sec and 1×10^{-9} sec, respectively. Thus the 56 AVP limits the resolution to

$$2\tau_{PM} \sim \sqrt{2(3 \times 10^{-10})^2} = 4.25 \times 10^{-10} \text{ sec} . \quad (15)$$

The combined effects of the phosphor and photomultiplier tube thus limit the overall resolution to

$$2\tau \sim \sqrt{(2\tau_S)^2 + (2\tau_{PM})^2} \sim 5 \times 10^{-10} \text{ sec} . \quad (16)$$

The actual resolution observed for prompt gamma rays was $2\tau = 5.70 \times 10^{-10}$ sec, as shown on Figure 7, and since these data were taken it has been reduced even further. Thus the experimental resolution is in quite good agreement with Equation 16. The resolution can also be limited by the time jitter caused by the varying limiter cut-off times which are associated with different size phototube anode pulses. This time jitter, however, can be eliminated by using an auxiliary circuit which will be described in Section E.

D. The Delayed Spectrum and Methods of Data Analysis

1. Log slope and centroid shift methods

Typical prompt and delayed time spectra are shown in Figure 7. Let P(x) denote the prompt spectrum as a function of the delay x, and let F(x) denote the delayed spectrum corresponding to positron annihilation with a mean life $\tau = 1/\lambda$. Then if P(x) and F(x) are normalized to unit area, it has been shown by Newton (45) that

$$F(x) = \lambda e^{-\lambda x} \int_{-\infty}^{x} e^{\lambda t} P(t) dt \quad . \tag{17}$$

Differentiating Equation 17 thus yields

$$\frac{dF(x)}{dx} = \lambda [P(x) - F(x)] \tag{18}$$

and

$$\frac{d[\ell n F(x)]}{dx} = -\lambda [1 + P(x)/F(x)] \quad . \tag{19}$$

Equation 18 indicates that F(x) will reach its maximum at its intersection with P(x), and this serves as a useful check on the consistency of the experimental data. Equation 19 shows that

$$\frac{d[\ell n F(x)]}{dx} = -\lambda = -\frac{1}{\tau} \text{ for } P(x) \ll F(x) \quad . \tag{20}$$

Thus, if the time resolution is good enough and the lifetime of the delayed radiation isn't too short, then one can obtain the mean life τ directly from the logarithmic slope of the delayed spectrum in the region for which $P(x) \ll F(x)$.

It has been shown by Bay (46) that the mean life is also given by the centroid shift between the delayed and prompt spectra. Thus

$$\tau = \bar{X}_F - \bar{X}_P \tag{21}$$

The centroid, $\bar{X}$, for either spectrum is given by

$$\bar{X} = \frac{\sum_i x_i y_i}{\sum_i y_i} \tag{22}$$

where x_i is the number, i, of the channel on the multichannel analyzer, and is proportional to the time delay; and y_i is the number of counts in channel i. The sums are over all of the channels. The standard error of the centroid, as indicated by Simms *et al.* (47), can be computed from

$$(\sigma_{\bar{x}})^2 \cong \frac{1}{(\sum_i y_i)^2} \sum_i y_i (x_i - \bar{X})^2 \quad . \tag{23}$$

While the log slope method makes use of only the small amount of the experimental data for which $P(x) \ll F(x)$, the

centroid shift method uses all of the data. Thus the centroid shift method is statistically much more accurate. Furthermore, the centroid is affected very little by a fairly uniform background, while the slope in the region where $P(x) \ll F(x)$ depends rather critically upon the background subtraction. The centroid position, however, is very sensitive to small drifts in the electronics, and it may change by as much as 5×10^{-11} sec ($\sim$1 channel) in one day. This, of course, could almost completely wash out shifts of the magnitude that are of interest. To overcome this handicap and still obtain the advantage of the better statistics inherent in this method, an automatic cycling procedure is used.

2. Cycling procedure

The experiment is programmed so that a reference time spectrum (e.g. positrons in aluminum) is accumulated in one half of a multichannel analyzer for 5 min. Then the reference source and the delayed source are automatically interchanged, and the delayed spectrum is accumulated in the other half of the analyzer for the next 5 min. The cycle is then repeated. In this way the instrumental drifts shift the prompt and the delayed spectra equally (assuming negligible drift in a 10 min period). A typical experiment lasts on the order of 100 or more cycles, and it is found that the lifetime for a given sample can be reproduced to within about $\pm$ 3 x 10^{-12} sec. It

should be noted here that most measurements are made relative to aluminum as a reference sample. It is assumed that the absolute lifetime, τ_{Al}, of positrons in aluminum is known. Then if $\Delta\tau$ is the centroid shift between the unknown time spectrum and the aluminum spectrum, the positron lifetime in the unknown sample is

$$\tau = \tau_{Al} + \Delta\tau \qquad (24)$$

It is inherently more difficult to measure absolute lifetimes directly, for reasons which will be explained in Section E-2.

The basic programmer circuit is shown in Figure 8. It consists of seven Sodeco preset counters (Type TCeF4PE) which are pulsed in parallel at 3 sec time intervals. As each counter reaches the preset number of counts, a pair of contacts closes, actuating an ac relay. These ac relays then perform the various switching functions indicated on the figure. When the seventh counter reaches the preset number of counts, two dc relays are closed. One relay actuates a cycle counting register, while the other opens the counter pulsing circuit and applies +200 volts to all of the counter reset coils. The two dc relays then open, and the cycle begins again. The programmer circuit includes a manual reset switch and an end stop switch, which can be opened so as to automatically halt the programmer at the end of the cycle then in progress.

The pulsing of the Sodeco counters is done with the

Figure 8. Programmer circuit. Seven Sodeco preset counters are pulsed in parallel at regular intervals. When a particular counter reaches its preset number of counts it closes an ac relay to perform one of the switching functions.

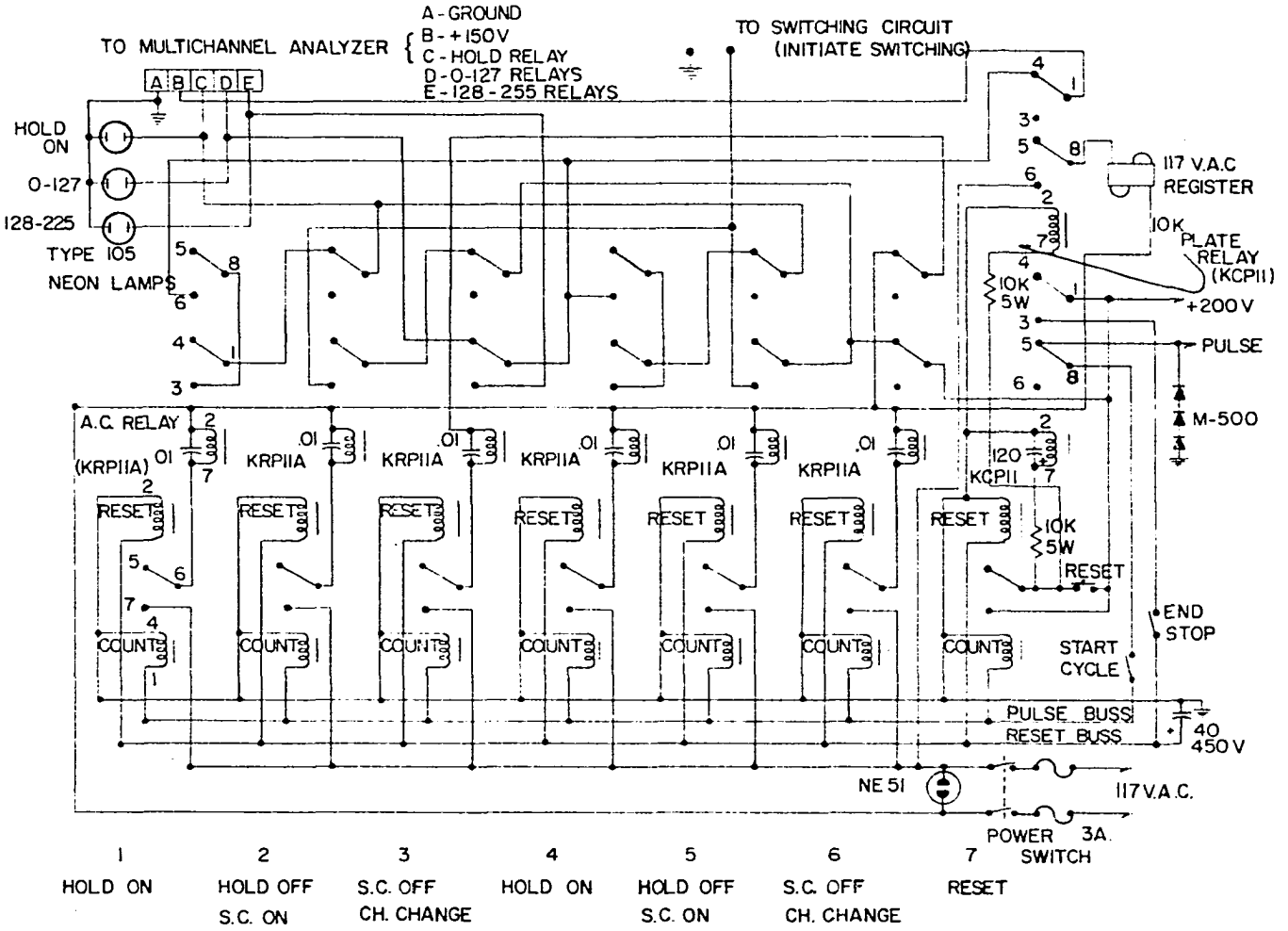
A - GROUND
B - +150V
C - HOLD RELAY
D - 0-127 RELAYS
E - 128 - 255 RELAYS
TO MULTICHANNEL ANALYZER
A B C D E
HOLD ON
0-127
128-225
TYPE 105 NEON LAMPS
TO SWITCHING CIRCUIT (INITIATE SWITCHING)
117 V.A.C REGISTER
10K
PLATE RELAY (KCP11)
+200 V
PULSE
M-500
A.C. RELAY (KRP11A)
.01
KRP11A
KCP11
120
10K 5W
RESET
COUNT
END
STOP
START CYCLE
PULSE BUSS
RESET BUSS
40 450 V
NE 51
117 V.A.C.
POWER SWITCH
3A.
1 HOLD ON
2 HOLD OFF S.C. ON
3 S.C. OFF CH. CHANGE
4 HOLD ON
5 HOLD OFF S.C. ON
6 S.C. OFF CH. CHANGE
7 RESET

circuit shown in Figure 9. A half-wave rectified ac signal is used to drive a 6J6 univibrator. The univibrator output is scaled down to thirty pulses per second with a General Electric 4SN1A3 binary unit. This triggers a unit which drives a Berkeley Model 705-A decimal counting unit and a Berkeley Model 730 preset decimal counting unit. The preset unit can be set so as to produce from one pulse every three seconds up to three pulses per second. (Ordinarily it is set for one pulse every three seconds.) This preset counting unit drives a 6SN7 univibrator. A plate relay in the univibrator circuit switches +200 volts on and off, thus supplying the pulses which actuate the Sodeco preset counters. The +200 volt supply is a simple voltage doubler circuit. The +300 and -150 volt supplies shown are used to power the various tubes in the timing circuit.

The switching of the analyzer is done by means of mercury relays (in the analyzer) which are turned on when a +150 volt supply (also in the analyzer) is connected to their coils. The +150 volt supply is connected to the proper mercury relay coils by using the programmer relays as switches. When pin B is connected to pin C, the hold mercury relay is switched on, causing the analyzer to accumulate data; when B is connected to D, the accumulation is in channels 0-127; and when B is connected to E the accumulation is in channels 128-255.

Figure 9. Timing circuit. This circuit supplies +200 volt pulses at regular intervals to actuate the Sodeco counters in the programmer circuit.

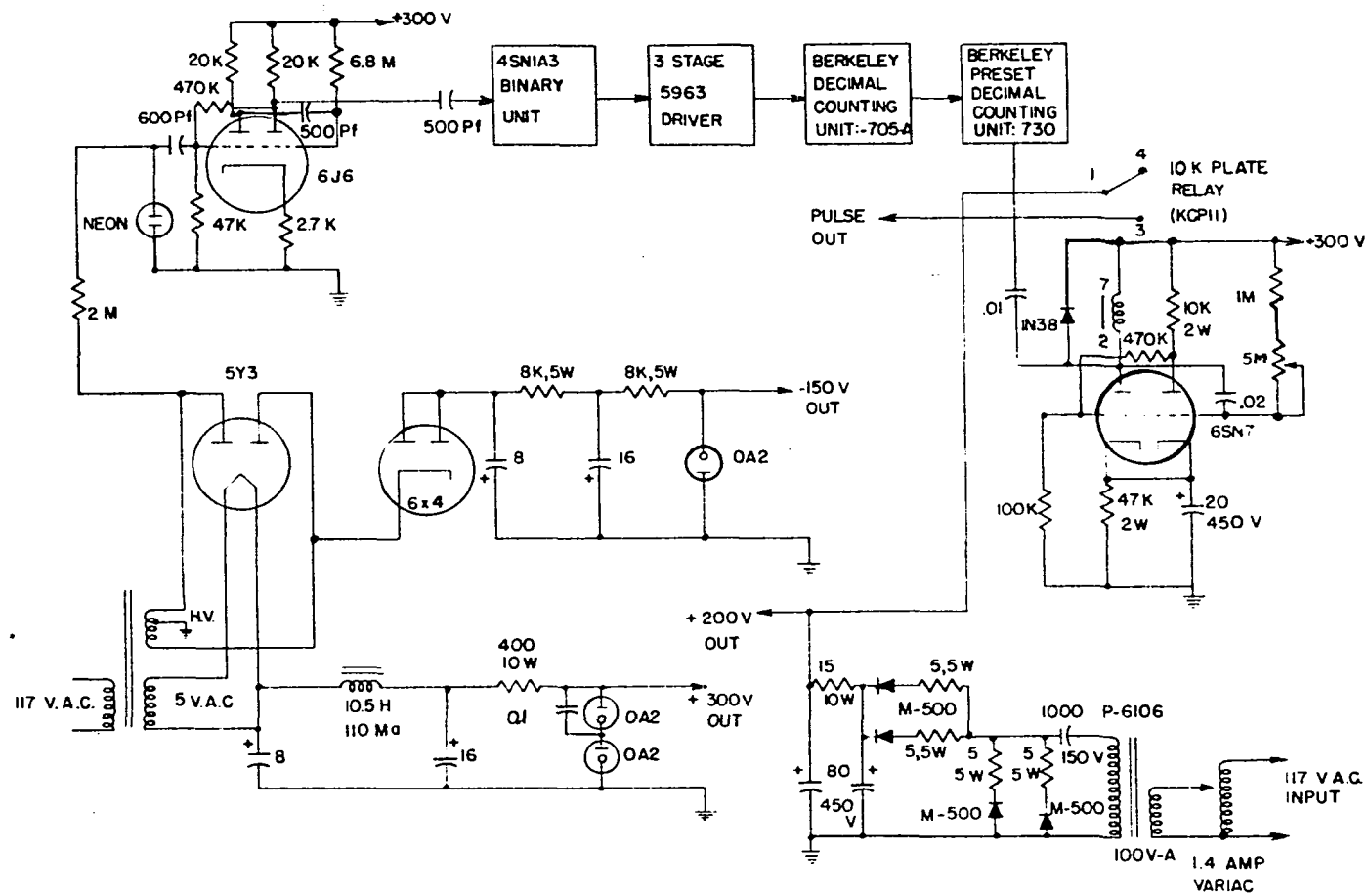
+300 V
20K
20K
6.8 M
470K
600 Pf
500 Pf
500 Pf
6J6
NEON
47K
2.7 K
2 M
4SN1A3 BINARY UNIT
3 STAGE 5963 DRIVER
BERKELEY DECIMAL COUNTING UNIT:-705-A
BERKELEY PRESET DECIMAL COUNTING UNIT: 730
10 K PLATE RELAY (KCP11)
PULSE OUT
+300 V
.01
IN38
10K 2W
1M
5M
470K
.02
6SN7
100K
47K 2W
20 450 V
5Y3
8K,5W
8K,5W
-150 V OUT
6x4
8
16
0A2
H.V.
117 V.A.C.
5 V.A.C
10.5 H 110 Ma
400 10W
.01
0A2
0A2
+300V OUT
+200 V OUT
15 10W
5,5W M-500
5,5W
1000 P-6106
5 5W
5 5W
150 V
80 450 V
M-500
M-500
100V-A
117 V.A.C. INPUT
1.4 AMP VARIAC

Three auxilliary circuits (each on a separate chassis) control the sample changing. These circuits are shown in Figure 10. At the proper time, +200 volts from the programmer is connected (for 3 sec) to the circuit labeled "Initiate Switching". This closes a KCP11 relay applying 117 v ac to A and A' of the mode control circuit.

The mode control circuit permits programming of either the sample changer or a coaxial relay. In the sample changing mode the ac voltage on A and A' is shunted to B and B' of the sample changer motor control circuit. In the cable changing mode the ac voltage on A and A' closes a KRP11A relay. This actuates a two position stepping relay, which in turn switches an external coaxial relay either on or off.

When operating in the sample changing mode, the ac voltage on B and B' actuates a relay which turns on a small motor. The samples to be interchanged are mounted on opposite edges of a disk which is driven by the motor through a speed reducer and a belt drive. As the disk starts to rotate, a cam turns on a microswitch. This microswitch keeps the motor turned on until the disk has rotated 180°, thus interchanging the samples. (The relay which starts the motor remains closed for only 3 sec, while the disk takes almost 30 sec to complete a half revolution.) To perform a centroid shift measuring experiment, the Sodeco counters 1 through 7 are preset to 1, 101, 102, 113, 213, 214, and 224 counts,

Figure 10. Switching circuits. A +200 volt signal from the programmer causes these circuits to either actuate the sample changer or switch a coaxial relay, depending upon the switch position in the mode control circuit.

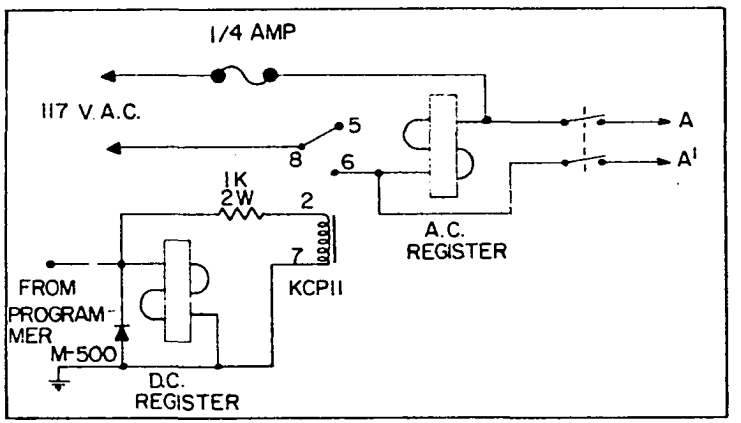

INITIATE SWITCHING

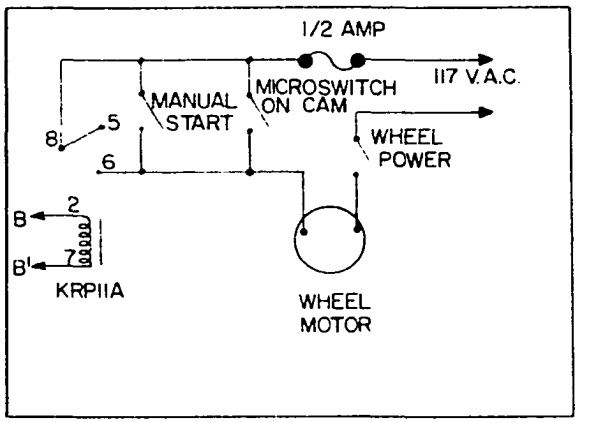

SAMPLE CHANGER MOTOR CONTROL

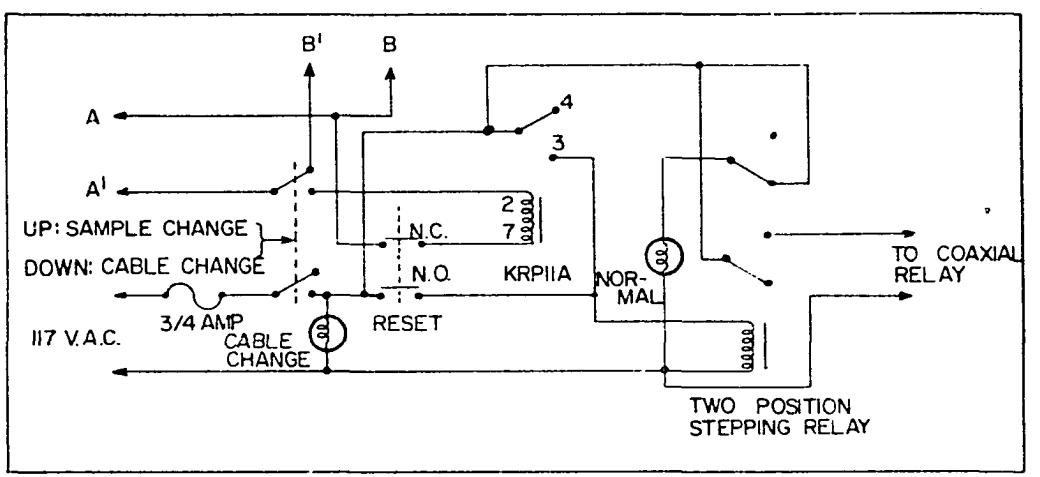

MODE CONTROL

respectively.

E. Auxilliary Circuits

1. Block circuit

A positron annihilation time spectrum always contains a small percentage of counts due to accidental coincidences. This background is actually due to two different types of event. One type of background is due to an accidental fast coincidence in the TAC accompanied by an accidental coincidence in the slow coincidence circuit. This type of background is completely random, and a correction for it can easily be made. Each detector is pointed at a separate Na^{22} source, and the two source-detector arrangements are isolated from each other. The source to detector distances are then adjusted to give the normal singles counting rates. The spectrum accumulated on the analyzer in a given time will then be just the random background that would be accumulated in a normal experiment lasting the same length of time.

A second type of background is due to events in which the roles of the 1.28 Mev gamma ray and the annihilation gamma ray are reversed. That is, the 1.28 Mev gamma ray enters the detector which normally detects annihilation radiation, and an annihilation gamma ray enters the detector which normally detects 1.28 Mev gamma rays. This type of event produces just as many fast coincidences in the TAC as the desired type of

event, but it is normally rejected by the energy selecting circuits. But if two annihilation events occur within a time less than the resolving time (~1 μsec) of the slow coincidence circuit, then it is possible that the correct amount of energy will be dissipated in each detector so as to produce an accidental slow coincidence. Thus, if two annihilation events occur within a period of about 1 μsec it is possible that an accidental slow coincidence gate pulse may occur. This pulse may then cause the analyzer to accept an event in which the roles of the 1.28 and 0.51 Mev gamma rays are reversed.

To reduce the type of background discussed above, a block circuit is used. This circuit is designed to reject all coincidence events which are preceded or followed within 2 μsec by any other event detected in either (or both) detector. A block diagram of this circuit is shown in Figure 11.

A circuit at the input of the TAC picks off two fast ($\sim 40 \times 10^{-9}$ sec) pulses every time there is an input pulse from either (or both) limiter. This pickoff circuit is shown in Figure 12, and it is a modification of a circuit described by Chaplin and Candy (48, p. 242). An input pulse cuts off a 1N100 diode, thus turning off the current in the primary of a pulse transformer. Two separate negative pulses are produced at the two pulse transformer secondaries, and their overshoots are suppressed by resistor and diode networks.

Each of the fast pulses from the pickoff circuit is

Figure 11. Block diagram of the block circuit. This circuit furnishes an anti-coincidence input to the slow coincidence circuit to block the analysis of events for which the roles of the 1.28 Mev gamma ray and the annihilation gamma ray are reversed.

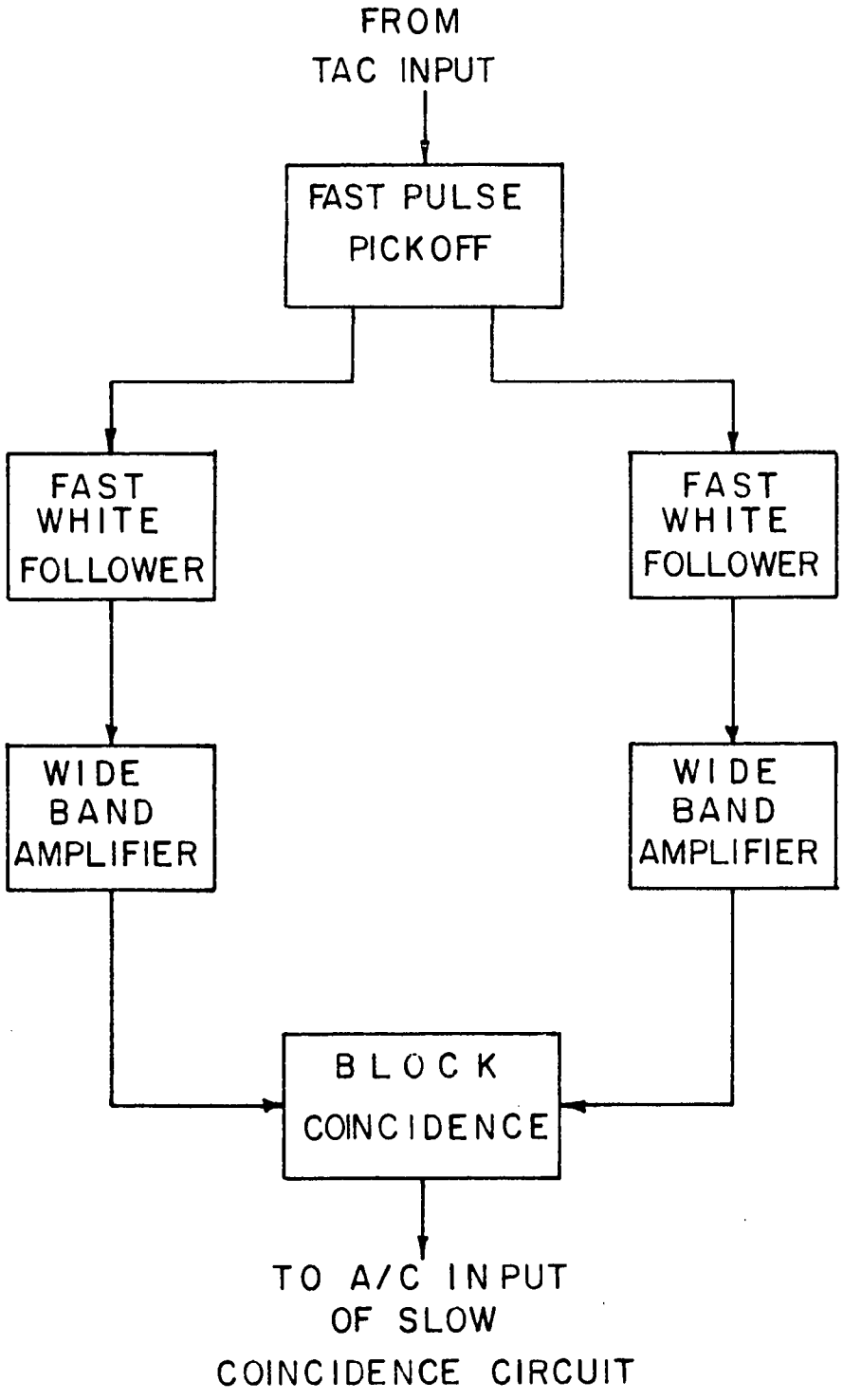
FROM
TAC INPUT
FAST PULSE
PICKOFF
FAST
WHITE
FOLLOWER
FAST
WHITE
FOLLOWER
WIDE
BAND
AMPLIFIER
WIDE
BAND
AMPLIFIER
BLOCK
COINCIDENCE
TO A/C INPUT
OF SLOW
COINCIDENCE CIRCUIT

Figure 12. Pickoff circuit. This circuit is part of the block circuit shown in Figure 11.

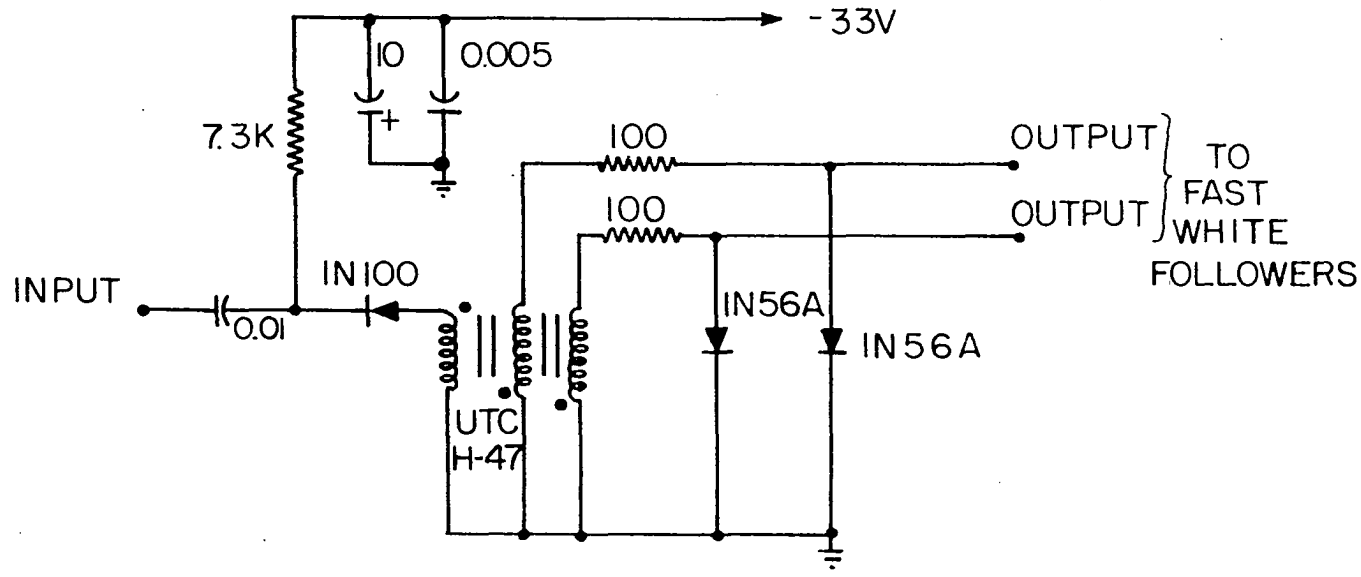
-33V
10
0.005
7.3K
100
OUTPUT
OUTPUT
TO
FAST
WHITE
FOLLOWERS
100
INPUT
IN100
0.01
IN56A
IN56A
UTC
H-47

fed to a separate fast White follower. Figure 13 shows the circuit diagram for the White followers. Each White follower is connected with 200 ohm cable to a Hewlett-Packard Model 460A wide band amplifier. The negative pulses (~5-10 volts) from the wide band amplifiers are connected with 200 ohm cable to the two inputs of a block coincidence circuit.

The block coincidence circuit is shown in Figure 14. The left-hand input triggers a univibrator which produces a 5 volt, 2 μsec negative pulse (block gate pulse). This pulse is coupled through an emitter follower (2N274) to one input of a Madey (39, pp. 973-974) type coincidence circuit. The right-hand input is coupled directly to the second input of the coincidence circuit. A coincidence output triggers an avalanche transistor (2N501) which produces a +5-10 volt pulse. This pulse is coupled through a two stage emitter follower to the anti-coincidence input of the slow coincidence circuit (described in Section B-3).

There is a slight time delay in the left-hand input to the block coincidence circuit, so that two otherwise simultaneous inputs do not cause a coincidence output. If, however, there is another input pulse on the right while the 2 μsec block gate pulse is still present, then a coincidence output will occur. This output then triggers the univibrator in the slow coincidence circuit (Figure 4), and the analyzer can not be gated on for the following 3 μsec. If the proper

Figure 13. Fast White follower. Two of these circuits are used to drive the wide band amplifiers used in the block circuit shown in Figure 11.

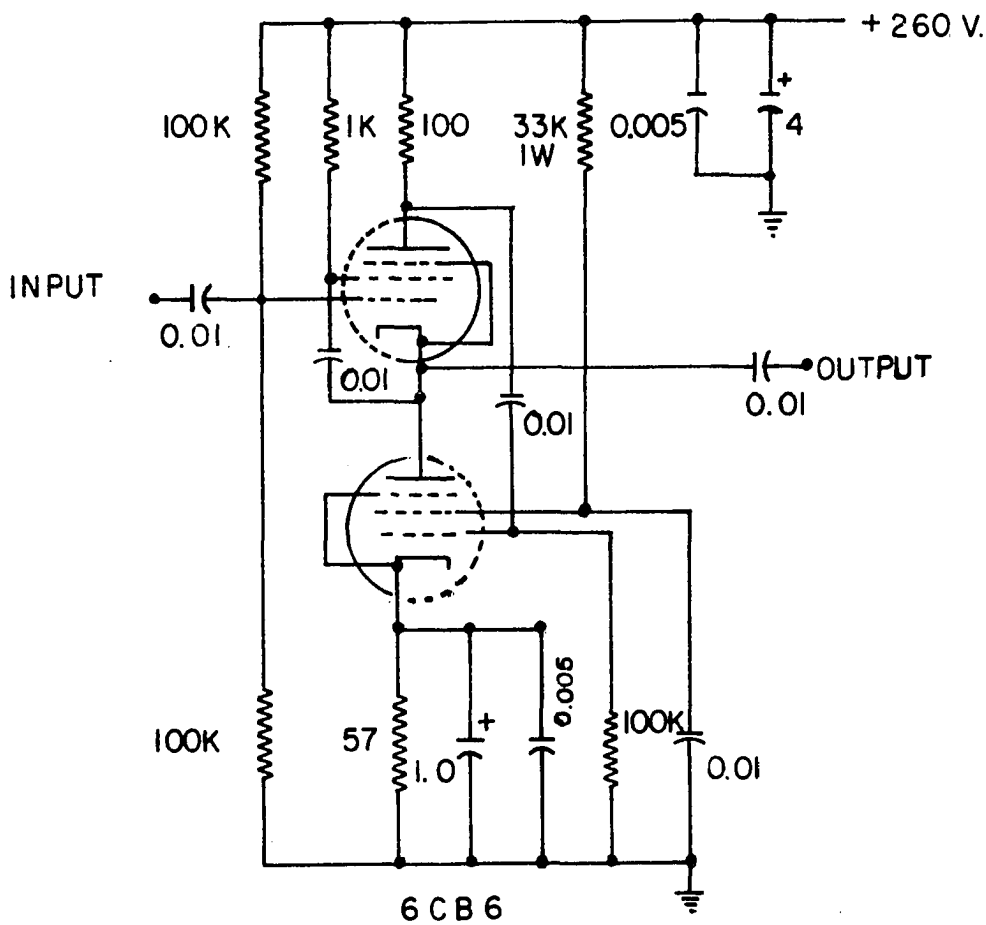
+ 260 V.
100K
1K
100
33K
1W
0.005
4
INPUT
0.01
0.01
0.01
OUTPUT
0.01
100K
57
1.0
0.006
100K
0.01
6CB6

Figure 14. Block coincidence circuit. This circuit produces an anti-coincidence input to the slow coincidence circuit any time two events are detected within a time interval of 2 μsec or less.

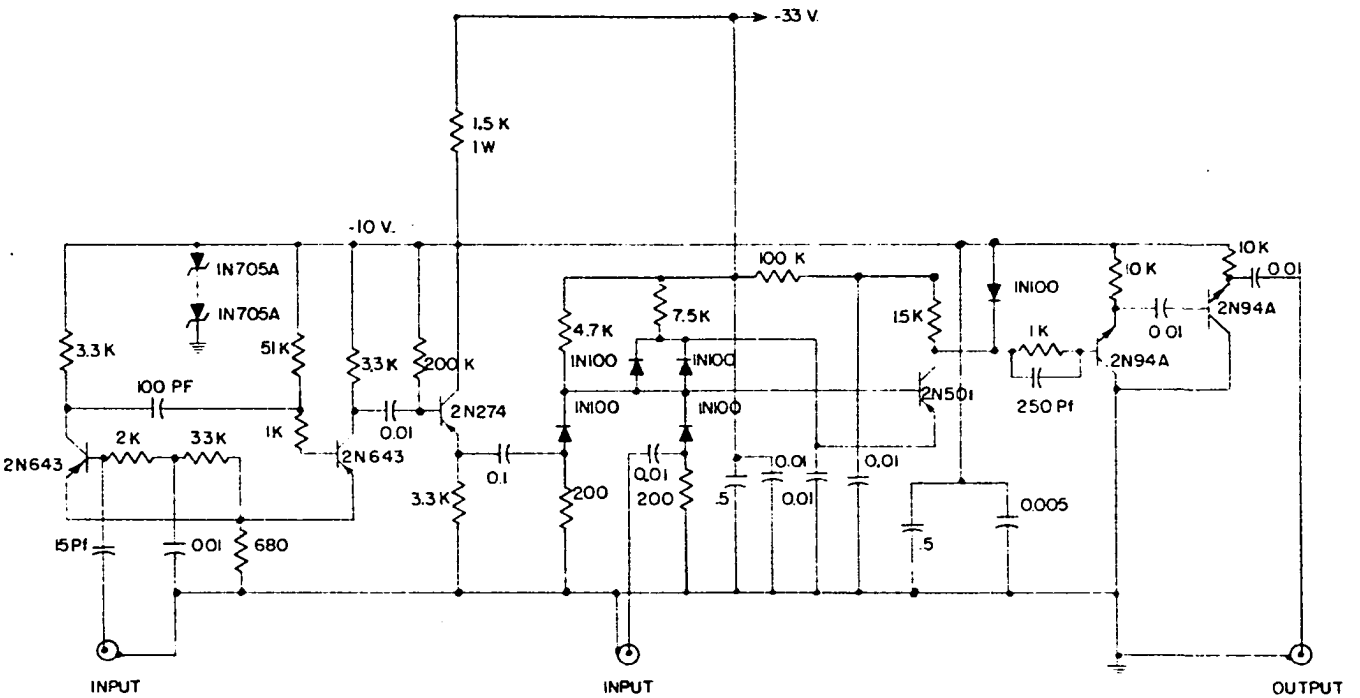
-33 V.
1.5 K
1W
-10 V.
IN705A
IN705A
3.3 K
51K
100 PF
2K
33K
1K
2N643
2N643
15Pf
.001
680
INPUT
3.3K
200 K
0.01
2N274
0.1
3.3K
4.7K
7.5K
100 K
IN100
IN100
IN100
IN100
200
0.01
200
.5
0.01
0.01
.5
0.005
15K
IN100
2N501
1K
250 Pf
10K
0.01
2N94A
0.01
2N94A
10K
0.01
INPUT
OUTPUT

amount of time delay is added between the linear amplifier and the pulse height selector in each of the energy selecting side channels, then the slow coincidence circuit will not gate a coincidence event into the analyzer if the event is preceded or followed within 2 μsec by any other event detected in either (or both) detector. (The amount of delay added to the side channels is such that the total circuit delay from a phototube to a coincidence input of the slow coincidence circuit is 2 μsec longer than the delay from the same phototube to the anti-coincidence input of the slow coincidence circuit.) It is thought that the block circuitry can resolve any two events that are separated in time by more than 0.05-0.06 μsec.

To check the performance of the block circuitry, the cable switching mode of the program circuit (Section D-2) was used. The time spectrum for positrons annihilating in aluminum was accumulated in the first half of the analyzer memory for five minutes with the block circuit connected. Then the anti-coincidence input to the slow coincidence circuit was disconnected, and the time spectrum was accumulated in the second half of the analyzer memory for five minutes. The cycle was then repeated. The run lasted for sixty-one cycles, and it was found that use of the block circuitry cut the total background rate to one-half of that present when the block circuitry was disconnected.

2. Centroid shift compensator

In order to obtain as high a fast coincidence counting rate as possible, it is desirable to use fairly wide windows in the energy selecting side channels (e.g. the upper one-third of the Compton distribution of the particular gamma ray being selected). Using a wide window, however, allows the limiter to be cut off with pulses of widely varying amplitudes. Since a small pulse takes longer to cut off the limiter than does a large pulse, the limiter output pulses corresponding to different input pulses will be delayed with respect to one another. This gives rise to a time jitter which broadens the time spectrum. Since one input to the TAC, channel 2, is artificially delayed from the other input, channel 1, a larger pulse in channel 1 results in a smaller TAC output, and a larger pulse in channel 2 results in a larger TAC output.

In order to use wide energy selection windows and yet avoid broadening of the time spectrum, a so-called centroid shift compensator circuit is used. The use of a compensating circuit was first suggested by Bell and Jørgensen (28, p. 654). As shown in Figure 15, pulses are tapped off at the outputs of the side channel amplifiers, attenuated, coupled through slow (~1 μsec) pulse transformers, and added to the (suitably delayed) output from the TAC. The pulse transformers are connected so that the pulses added from channel 1 are of the same polarity as the TAC output, while the pulses added from

Figure 15. Centroid shift compensator. This circuit eliminates the time jitter caused by the varying limiter cut-off times associated with pulses of many different amplitudes.

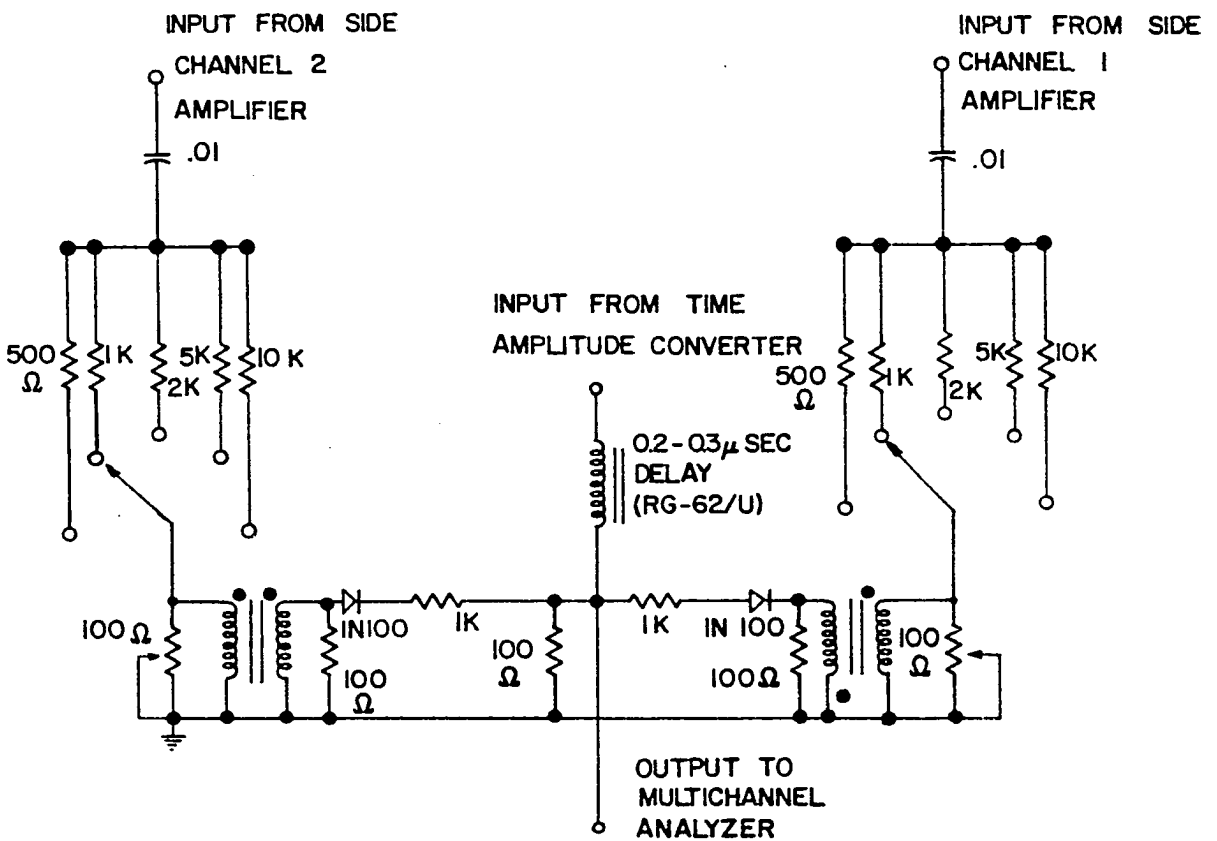
INPUT FROM SIDE
CHANNEL 2
AMPLIFIER
.01
500 Ω
1 K
5K
2K
10 K
INPUT FROM TIME
AMPLITUDE CONVERTER
0.2-0.3μ SEC
DELAY
(RG-62/U)
INPUT FROM SIDE
CHANNEL 1
AMPLIFIER
.01
500 Ω
1K
2K
5K
10K
100 Ω
IN100
1K
100 Ω
100 Ω
1K
IN 100
100Ω
100 Ω
OUTPUT TO
MULTICHANNEL
ANALYZER

channel 2 are of opposite polarity. The attenuation in each channel is adjusted so that the amplitude of the pulse to the multichannel analyzer is independent (to first order) of the energy lost in either detector over the range of energies to be selected. The main advantage of this particular compensation circuit lies in its simplicity. No vacuum tubes or other active devices need be used.

As a check on the compensator circuit, a prompt (Co^{60}) time spectrum was run first with compensation and then (on the following day) without compensation. The time resolution with compensation was $2\tau = 5.70 \times 10^{-10}$ sec, while without compensation it was $2\tau = 6.87 \times 10^{-10}$ sec. Thus, use of the compensator results in almost a 20% improvement in the time resolution.

It should be noted that use of the compensator is particularly important when making absolute lifetime measurements using the centroid shift technique. Since the prompt source (Co^{60}) has a different energy spectrum than the delayed source (Na^{22}), the average height of the pulses cutting off the limiters may be different for the two sources. This can lead to spurious centroid shifts of several times 10^{-11} sec, and thus can cause serious errors in the measured lifetimes. Use of the proper amount of compensation, however, can practically eliminate this effect.

In Figure 16 is shown a complete block diagram of the

Figure 16. Complete block diagram of the electronics

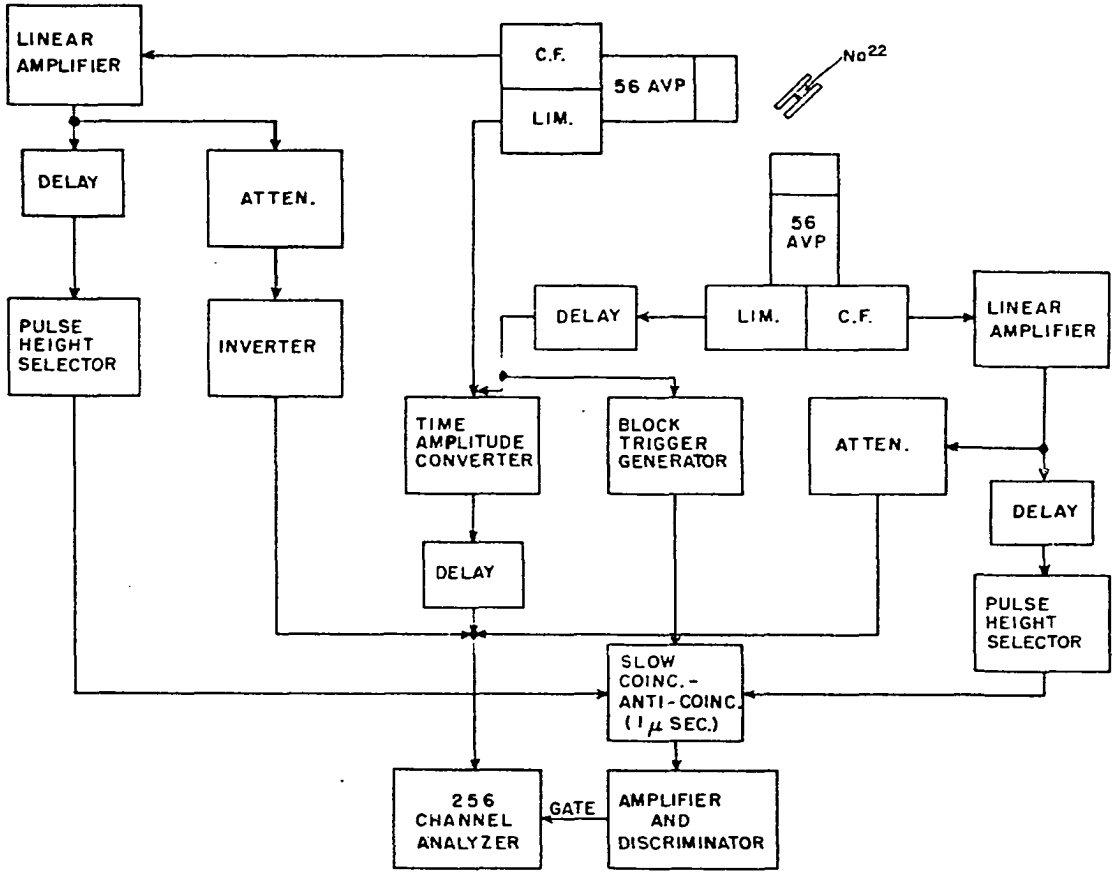
LINEAR AMPLIFIER
C.F.
LIM.
56 AVP
Na22
DELAY
ATTEN.
56 AVP
PULSE HEIGHT SELECTOR
INVERTER
DELAY
LIM.
C.F.
LINEAR AMPLIFIER
TIME AMPLITUDE CONVERTER
BLOCK TRIGGER GENERATOR
ATTEN.
DELAY
DELAY
PULSE HEIGHT SELECTOR
SLOW COINC. - ANTI-COINC. (1 μ SEC.)
256 CHANNEL ANALYZER
GATE
AMPLIFIER AND DISCRIMINATOR

electronics, including the block circuit, the compensator circuit, and the necessary delays.

F. Calibration Procedure

The TAC is calibrated by determining the centroid of a time spectrum (from positrons annihilating in aluminum) as a function of the length of RG-62/U cable inserted between one of the limiters and the TAC. Each calibration cable was cut from the same spool of cable and its length measured. A signal propagation velocity of 2.43×10^{10} cm/sec was then used to compute their electrical lengths. All of the cables should have the same propagation velocity, and this is not expected to deviate from the assumed value by more than a few percent. It should be noted that a 3% error in the propagation velocity could cause an error of $\sim 6 \times 10^{-12}$ sec in an absolute lifetime measurement, but in comparing relative lifetimes that differ by only a few times 10^{-11} sec the error would be less than 1×10^{-12} sec.

A typical calibration curve is shown in Figure 17. The centroid of the time spectrum is plotted against the net delay in one of the side channels, and the straight line is a least squares fit to the experimental data. As can be seen, the calibration curve is quite linear over a range of about 5 nanoseconds. On either side (not shown) of this region the slope becomes less steep. In making the actual lifetime

Figure 17. A typical time calibration curve

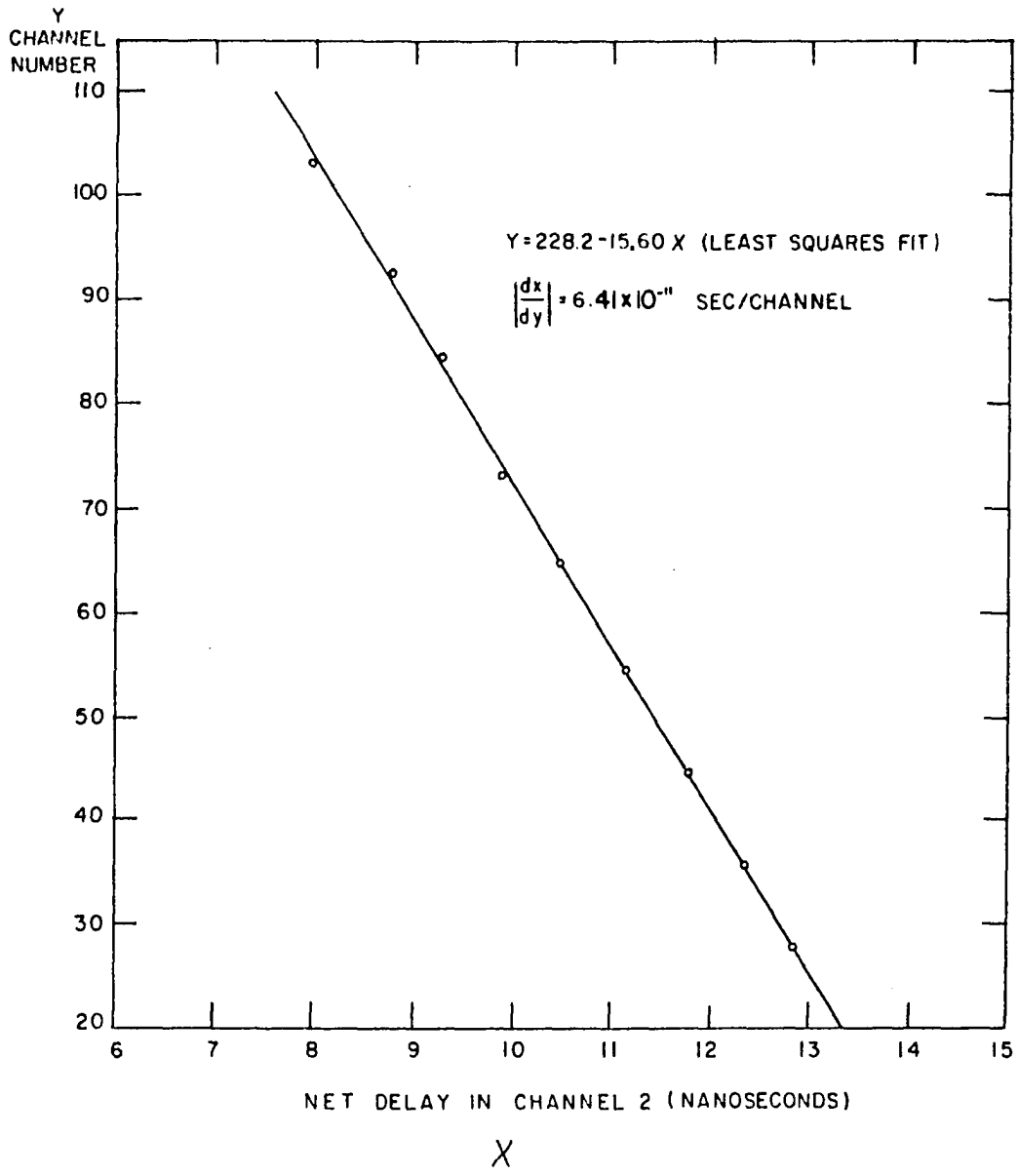
Y
CHANNEL
NUMBER
110
100
90
80
70
60
50
40
30
20
6
7
8
9
10
11
12
13
14
15
Y = 228.2 - 15.60 X (LEAST SQUARES FIT)
|dx/dy| = 6.41 x 10⁻¹¹ SEC/CHANNEL
NET DELAY IN CHANNEL 2 (NANOSECONDS)
X

measurements the net delay is adjusted so that the centroids of the time spectra fall near the center of the linear region.

A normalization procedure is used to eliminate errors due to drifts in the electronics during the calibration run. The spectrum for a reference delay is accumulated in half of the analyzer memory for two minutes, and then the spectrum for one of the other delays is accumulated in the other half of the analyzer memory for four minutes. Finally, the spectrum for the reference delay is accumulated in the first half of the analyzer memory for another two minutes. Each of the other delays is compared with the reference delay in this same manner, and the data are normalized to a fixed value for the centroid corresponding to the reference delay.

A calibration curve like that shown in Figure 17 is usually run before a series of experiments. Before and after each individual experiment, however, a four point calibration (using the normalization procedure) is run. A least squares fit is made for each of these runs, and the average of the two is used as the calibration for the experiment. The calibration is usually constant to within one or two percent for a week or more at a time, although occasional deviations of several percent may occur.

G. Experimental Errors

The three main sources of random errors in the measured relative lifetimes are: the statistical uncertainty in the

measured centroid shift, the calibration error, and the positioning error. The standard error in the computed centroids can readily be calculated from Equation 23, and the error in the centroid shift will then be just the square root of the sum of the squares of the errors in the two separate centroids. For 100 cycle runs this error was always found to be less than $\pm$ 2 x 10^{-12} sec. As indicated in Section F, the calibration can be determined with less than a 2% error (neglecting the systematic error due to the uncertainty in the cable propagation velocity, as this shifts all of the relative measurements by approximately the same amount of time). Since none of the measured centroid shifts are much longer than 1×10^{-10} sec, the calibration error should be less than $\pm$ 2×10^{-12} sec.

Because of the very short times being measured, differences in gamma ray transit times can also lead to experimental errors. Thus when data is being accumulated with the unknown sample, its source must be in exactly the same position as was the source for the reference sample when its data was being accumulated. If the positioning error is to be kept to $\pm$ 1 x 10^{-12} sec, then the sources must be lined up to within $(1/\sqrt{2})(1 \times 10^{-12}$ sec$)(3 \times 10^{10}$ cm/sec$)(1/2.54)$ in./cm $\cong$ 0.008 in. (The factor $1/\sqrt{2}$ is included because the detectors are 90° apart. If they were 180° apart the factor would be 1/2.) It is believed that the two sources can be positioned with this accuracy. Both pieces of a sample are

carefully measured with a micrometer before the Na^{22} source is sandwiched between them, and thus the distance from the surface of the sample to the source is accurately known. Before a run is begun the reference source and the unknown source can then be lined up using a surface feeler gauge.

The total random error in a relative lifetime measurement should then be the square root of the sum of the squares of the three errors mentioned above. Thus

$$\begin{aligned} e &= \pm \sqrt{(2)^2 + (2)^2 + (1)^2} \times 10^{-12} \text{sec} \\ &= \pm 3 \times 10^{-12} \text{ sec} \quad . \end{aligned} \tag{25}$$

As a check on the errors involved in the relative lifetime measurements, eight separate runs were made comparing the mean lives of positrons in two different aluminum samples. Between some of these runs the two samples were removed and then repositioned. The result for each of the eight runs is shown in Figure 18. The weighted average of the eight runs yielded a lifetime difference of 2×10^{-12} sec, and the average deviation of the individual runs from this value was $\pm 3 \times 10^{-12}$ sec.

Figure 18. Results of null experiments. Eight separate runs were made comparing the mean lives of positrons in two different aluminum samples.

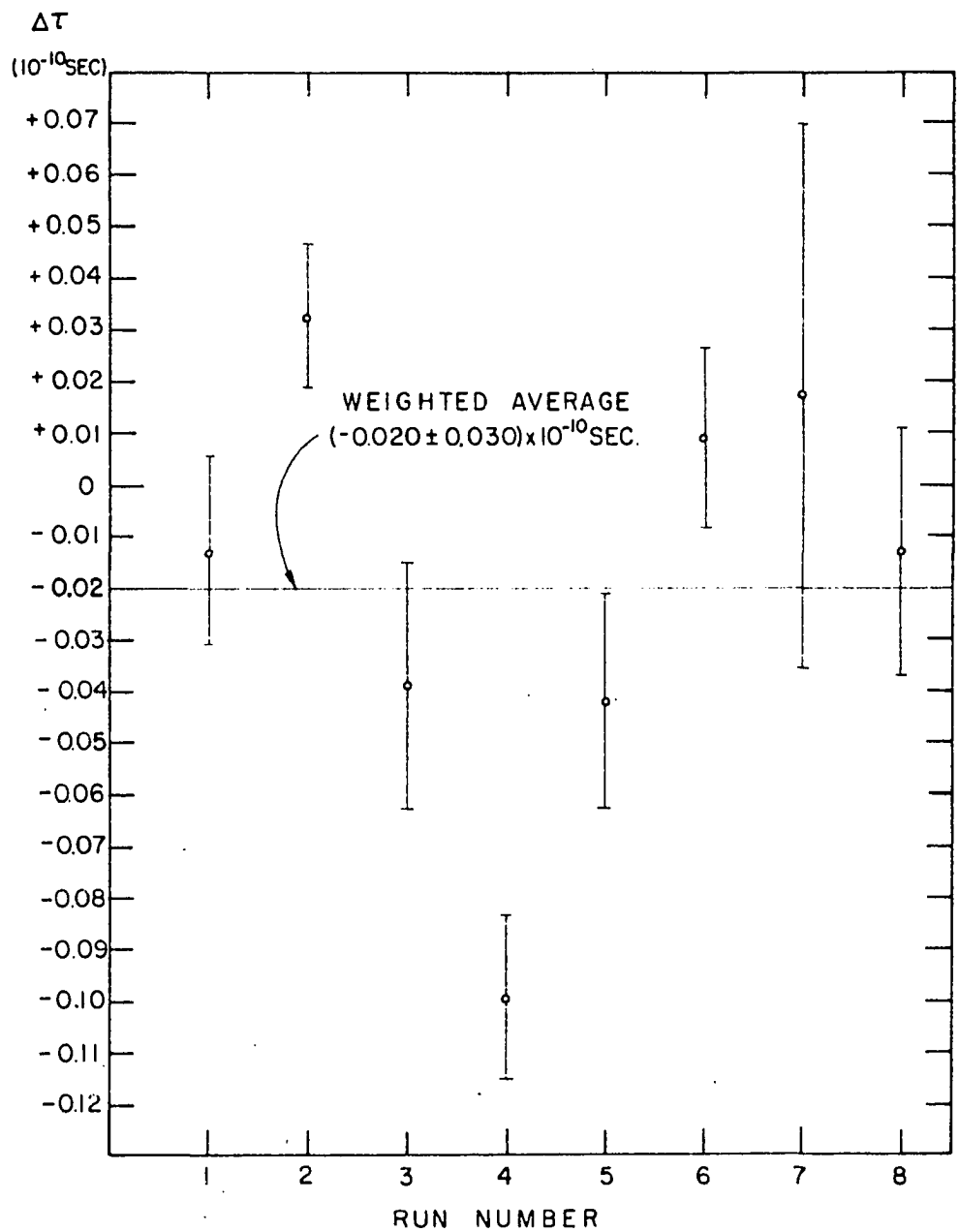
Δτ
(10⁻¹⁰SEC)
+0.07
+0.06
+0.05
+0.04
+0.03
+0.02
+0.01
0
-0.01
-0.02
-0.03
-0.04
-0.05
-0.06
-0.07
-0.08
-0.09
-0.10
-0.11
-0.12
WEIGHTED AVERAGE
(-0.020 ± 0.030)x10⁻¹⁰SEC.
1
2
3
4
5
6
7
8
RUN NUMBER

IV. EXPERIMENTAL RESULTS

A. Absolute Positron Lifetime in Aluminum

Most of the positron lifetimes measured in the present investigation are relative to the positron lifetime in aluminum. In order to convert these measurements into absolute lifetimes (using Equation 24) it is necessary to know the absolute lifetime of positrons in aluminum. For this reason the compensator circuit was carefully adjusted to eliminate spurious centroid shifts, and the centroid shift for positrons annihilating in aluminum relative to a Co^{60} prompt spectrum was measured. The result of a series of such runs was a centroid shift of $(2.24 \pm 0.05) \times 10^{-10}$ sec. The time spectra for these runs (with the random background subtracted) are shown in Figure 7. It is seen that the aluminum data cannot be fitted by a single exponential. They can, however, be fitted with two exponentials, one corresponding to a mean life $\tau_1 = 2.11 \times 10^{-10}$ sec with an intensity of $\sim 94\%$, and a second one with a mean life $\tau_2 = 3.81 \times 10^{-10}$ sec and an intensity of $\sim 6\%$. If f is the fraction of the τ_2 component present, then it is easily shown that the expected centroid shift for the above experiment is $(1 - f)\tau_1 + f\tau_2 = .94(2.11 \times 10^{-10} \text{ sec}) + .06(3.81 \times 10^{-10} \text{ sec}) = 2.21 \times 10^{-10}$ sec, and this is in good agreement with the measured shift of $(2.24 \pm 0.05) \times 10^{-10}$ sec.

Table 1. Positron mean lives in aluminum

Group	τ_1 (10^{-10} sec)	τ_2 (10^{-10} sec)	Date
Present work	2.11 ± 0.10	3.81 (6%)	----
Bell and Jørgensen (28)	1.9 ± 0.2	3.85 (6.5%)	1960
Jones (49)	2.40 ± 0.15	--	1959
Bisi et al. (29)	2.57 ± 0.06	--	1960
Gerholm (50)	2.5 ± 0.3	10 ± 4	1956

In Table 1 are shown the results of the present investigation along with those of other investigators. Since the measurements of Jones and Bisi et al. were made only with centroid shift techniques they did not see the τ_2 component, and their results should be compared with the composite lifetime of $(2.24 \pm 0.05) \times 10^{-10}$ sec found in the present investigation.

It can be seen that the results of the present work agree quite well with those quoted by most of the other investigators. Bisi et al., however, quote the smallest error, and their results are not in good agreement with the results of the present investigation. When making an absolute measurement, however, it is possible to get a spurious centroid shift of several times 10^{-11} sec, because the prompt (Co^{60}) and the delayed (Na^{22}) sources do not have the same energy spectra.

The present investigation utilized a compensation circuit to eliminate this shift. In order to determine the magnitude of the spurious shift, the aluminum experiment was rerun with the compensation circuit purposely disconnected. The result of this measurement was a centroid shift of $(2.56 \pm 0.05) \times 10^{-10}$ sec, which agrees very well with the (presumably uncompensated) result of Bisi et al. Thus it is obvious that compensation is very important when attempting absolute lifetime measurements with the centroid shift technique.

As mentioned by Bell and Jørgensen (28, p. 657), Gerholm has found that part of the tail on his aluminum spectrum was due to pile-up effects. He has, however, not been able to eliminate it completely, and presumably his value of τ_2 is now in better agreement with that found by the other two groups listed in Table 1. A possible explanation of the τ_2 component has been given by Gerholm (50, pp. 543-546). He assumes that positronium is formed in the aluminum, and that the τ_1 lifetime is given by

$$\frac{1}{\tau_1} = \frac{1}{\tau_{pos}} + \frac{1}{\tau_{free}} \qquad (26)$$

where τ_{pos} is the positronium lifetime in the limit of rapid triplet to singlet conversion (as given by Equation 8), and τ_{free} is the lifetime for the competing process of annihilation of the bound positron with an external free electron. He also

assumes that a few of the positronium atoms reach thermal energies. In this case triplet to singlet conversion can no longer occur, because all of the low energy electron states are already occupied. As far as the triplet state is concerned, then, one is left with only the free electron annihilation process. Hence

$$\tau_2 = \tau_{free} \tag{27}$$

While Gerholm's explanation of the τ_2 component is very tempting, it has been pointed out by Bell and Jørgensen (28, p. 663) that this explanation is contradicted by the results on angular correlation of annihilation quanta as reported by Berko and Plaskett (23). If thermalized positronium is present it should show up as a narrow component in the angular distribution, corresponding to annihilation of the positrons in the thermalized positronium atoms. Unfortunately this narrow component is definitely not present, and thus the τ_2 component in aluminum remains unexplained.

B. Positron Lifetimes in the Rare Earth Metals

All of the rare earths have a core configuration consisting of the inert xenon configuration plus a number of 4f electrons (which varies from 0 in lanthanum up to 14 in lutetium). In the normal room temperature phase all of the rare earth metals are trivalent except europium and ytterbium,

which are divalent. Scandium and yttrium (both trivalent) are often grouped with the rare earths because they occur in the same group (III) in the periodic table, and because they have properties very similar to the rare earths.

Positron mean lives were measured for all of the stable rare earths as well as for scandium and yttrium. The 5-10 μC positron source ($Na^{22}Cl$ in distilled water; ~ 1 μC/μliter) was deposited between two pieces of 0.25 mil aluminum foil and dried with a heat lamp. The source was then sandwiched between two polished pieces of the rare earth metal to be studied. The aluminum foil was necessary because some of the rare earths react quite strongly with water. It is estimated that no more than a few percent of the positrons annihilate in the aluminum, and this would cause an almost constant error of no more than 1% in the measured mean lives. Because it reacts rapidly with the atmosphere, the europium sample was prepared in a dry box which was evacuated and then filled with dry nitrogen. The finished sample was then sealed in paraffin to exclude the atmosphere.

The lower curve in Figure 19 is a plot of r_s' versus the atomic number of the rare earth. The r_s values computed from Equation 4 have been reduced slightly by subtracting the ionic volume (from which the positrons are assumed to be excluded) from the atomic volume. It can be seen that r_s' is approximately constant ($\bar{r}_s' = 2.47$) for all of the trivalent

Figure 19. Variation of r_s' and τ with z for the rare earth metals. The lower curve shows how the radius of the unit conduction electron sphere (corrected for the excluded volume of the ion) varies with z, while the upper curve shows the measured positron mean lives for the rare earth metals.

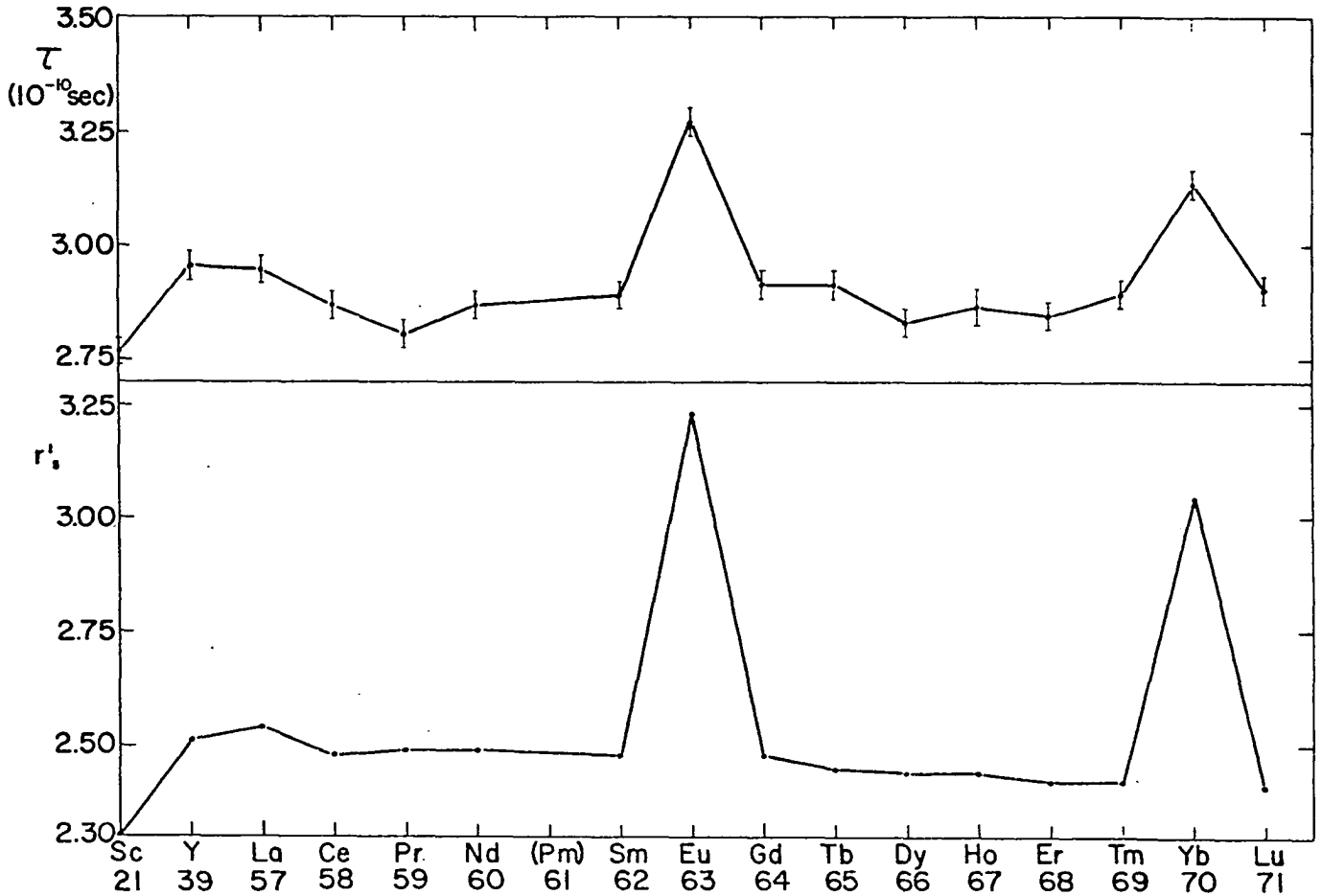
3.50
τ
(10⁻¹⁰sec)
3.25
3.00
2.75
3.25
r'₂
3.00
2.75
2.50
2.30
Sc 21
Y 39
La 57
Ce 58
Pr 59
Nd 60
(Pm) 61
Sm 62
Eu 63
Gd 64
Tb 65
Dy 66
Ho 67
Er 68
Tm 69
Yb 70
Lu 71

rare earths, but it is appreciably larger for europium and ytterbium. The value of r_s' is somewhat smaller for scandium because it has an appreciably smaller atomic volume than the other trivalent rare earths.

The upper curve in Figure 19 shows the positron lifetimes measured experimentally (assuming a composite positron lifetime in aluminum of 2.21×10^{-10} sec). There is obviously a definite correlation between the r_s' values and the measured lifetimes. The average lifetime for all of the trivalent rare earths (except scandium) is 2.885×10^{-10} sec, and the average deviation from this value is $\pm 0.035 \times 10^{-10}$ sec. The number of 4f electrons, however, varies from 0 in lanthanum to 14 in lutetium, and thus one can conclude that the 4f electrons do not participate in the annihilation process. The much smaller density of conduction electrons in the divalent rare earths, however, does give rise to an appreciably longer positron mean life, while the somewhat higher conduction electron density in scandium leads to a shorter positron mean life.

In Figure 20 the measured annihilation rates for the rare earth metals as well as Bell and Jørgensen's (28) results for the alkali metals are plotted versus r_s'. Bell and Jørgensen's data were used to compute the composite lifetime, $(1-f)\tau_1 + f\tau_2$, which would be measured in a centroid shift experiment for each of the alkali metals. These lifetimes were then normalized to a positron lifetime of 2.21 x

Figure 20. Annihilation rate versus r_s' for the rare earth and alkali metals. The annihilation rates measured for the rare earth metals in the present investigation together with Bell and Jørgensen's (28) values for the alkali metals (normalized to $\tau_{Al} = 2.21 \times 10^{-10}$ sec) are shown. A smooth curve is drawn through the experimental points, and various theoretical curves are shown for comparison.

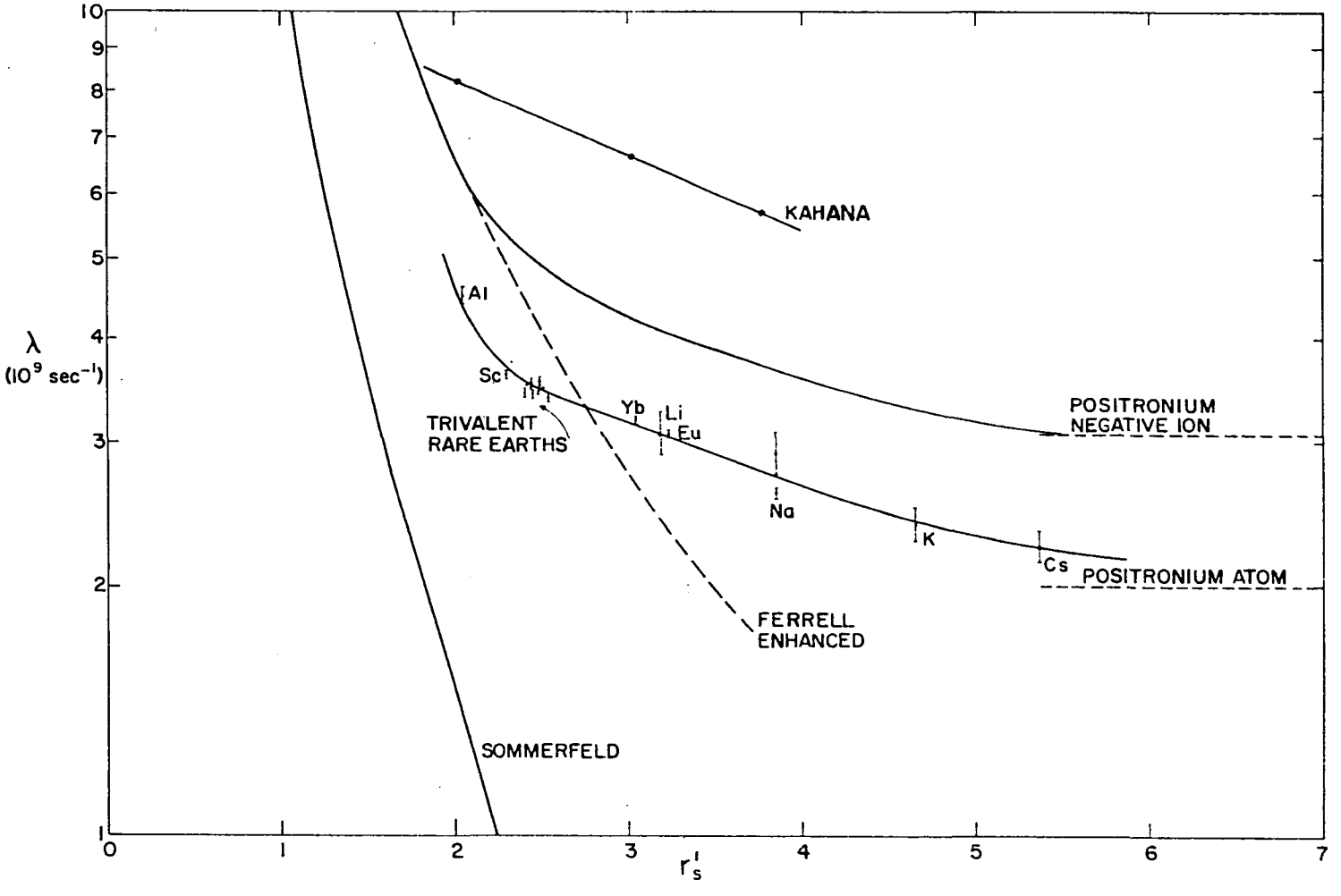
λ
(10⁹ sec⁻¹)
10
9
8
7
6
5
4
3
2
1
0
1
2
3
4
5
6
7
r_s'
KAHANA
Al
Sc
Yb
Li
Eu
TRIVALENT
RARE EARTHS
POSITRONIUM
NEGATIVE ION
Na
K
Cs
POSITRONIUM ATOM
FERRELL
ENHANCED
SOMMERFELD

10^{-10} sec in aluminum, and the annihilation rates computed from these normalized lifetimes are the ones plotted in the figure. The positron lifetime in sodium was also measured during the present investigation, and the result of this measurement is the lower one of the two points marked Na on the figure. (The sodium sample, being very reactive, was prepared in the same manner as the europium sample described previously.) Various theoretical curves are also included on the figure.

It can be seen that the experimental data (including the alkali metals) lie on a fairly smooth curve, but they are not fit at all well by any of the theoretical curves. (Actually, the data are fitted quite well by $\lambda \propto (r_s')^{-1/2}$.) The Sommerfeld theory is way off, and while the Kahana theory seems to give approximately the correct variation of λ with r_s', the predicted annihilation rate is about a factor of 2 too large. Ferrell expected his theory to hold only for high electron densities (small r_s'), and he expected that for low electron densities the annihilation rate would approach that of the positronium negative ion (two electrons bound to a positron). This is indicated in a qualitative manner by the solid curve which is arbitrarily drawn so as to be tangential to the enhanced curve at $r_s' = 2.5$ and to be tangential to the positronium ion rate at $r_s' = 5.5$. It would seem, however, that the actual annihilation rates at

low electron densities are more nearly tangential to the positronium atom rate.

It should be noted that all of the theories of positron annihilation rates assume that annihilation takes place only with the valence electrons. It is known from the measurements of the angular correlation of annihilation photons, however, that some core annihilation does take place. In principle the percentage of core annihilation can be determined from an angular correlation experiment for each case, and the measured annihilation rates can then be adjusted accordingly. The actual angular correlation experiments on the rare earths, however, yield ambiguous results on this point,* and thus a reliable correction for core annihilation can not be made. If the elements are grouped into families whose members have similar electron core configurations, then perhaps the annihilation rates for any one family will be a smooth function of r_s'. The alkali metals have only the valence electron outside of an inert gas configuration, and the rare earth metals have only the valence electrons outside of a core consisting of an inert gas configuration plus the well shielded 4f electrons. Thus the alkali metals and the rare earth metals belong to a family of the type discussed above, and indeed

---

*Gustafson, D., Department of Physics, Iowa State University of Science and Technology, Ames, Iowa. Angular correlation of photons from positron annihilation in rare earth metals. Private communication. 1962.

their annihilation rates do vary quite smoothly with r_s'. [Note that zinc has almost the same r_s' as scandium, while its annihilation rate (29) is about 40% greater. Zinc, however, has ten 3d electrons (in addition to the valence electrons) outside of an inert gas configuration, and these electrons may appreciably increase the annihilation rate over that due to the valence electrons alone.]

The time spectra for scandium, cerium, europium, and ytterbium are shown in Figures 21-24. The time spectra for all of the other trivalent rare earths are quite similar to that of cerium and are not shown. As can be seen, the positron mean lives obtained from the log slopes of the time spectra are in quite good agreement with the more accurate centroid shift determinations.

C. Positron Lifetimes in the Sodium Tungsten Bronzes

The centroid shift technique was used to determine the positron mean lives in metallic sodium tungsten bronzes (Na_xWO_3) with x values of 0.51, 0.717, and 0.835. The samples were made by depositing $Na^{22}Cl$ in 0.5 normal HCl on a polished piece of Na_xWO_3. The source was then evaporated to dryness and covered with another polished piece of Na_xWO_3. The results of these measurements are given by the circles in Figure 25.

If it is assumed that the positron lifetime in Na_xWO_3 depends upon the density of conduction electrons furnished by

Figure 21. Time spectrum of positron annihilation in scandium. The positron mean life obtained from the centroid shift measurement is $(2.77 \pm 0.03) \times 10^{-10}$ sec, using a time calibration of 7.465×10^{-11} sec/channel.

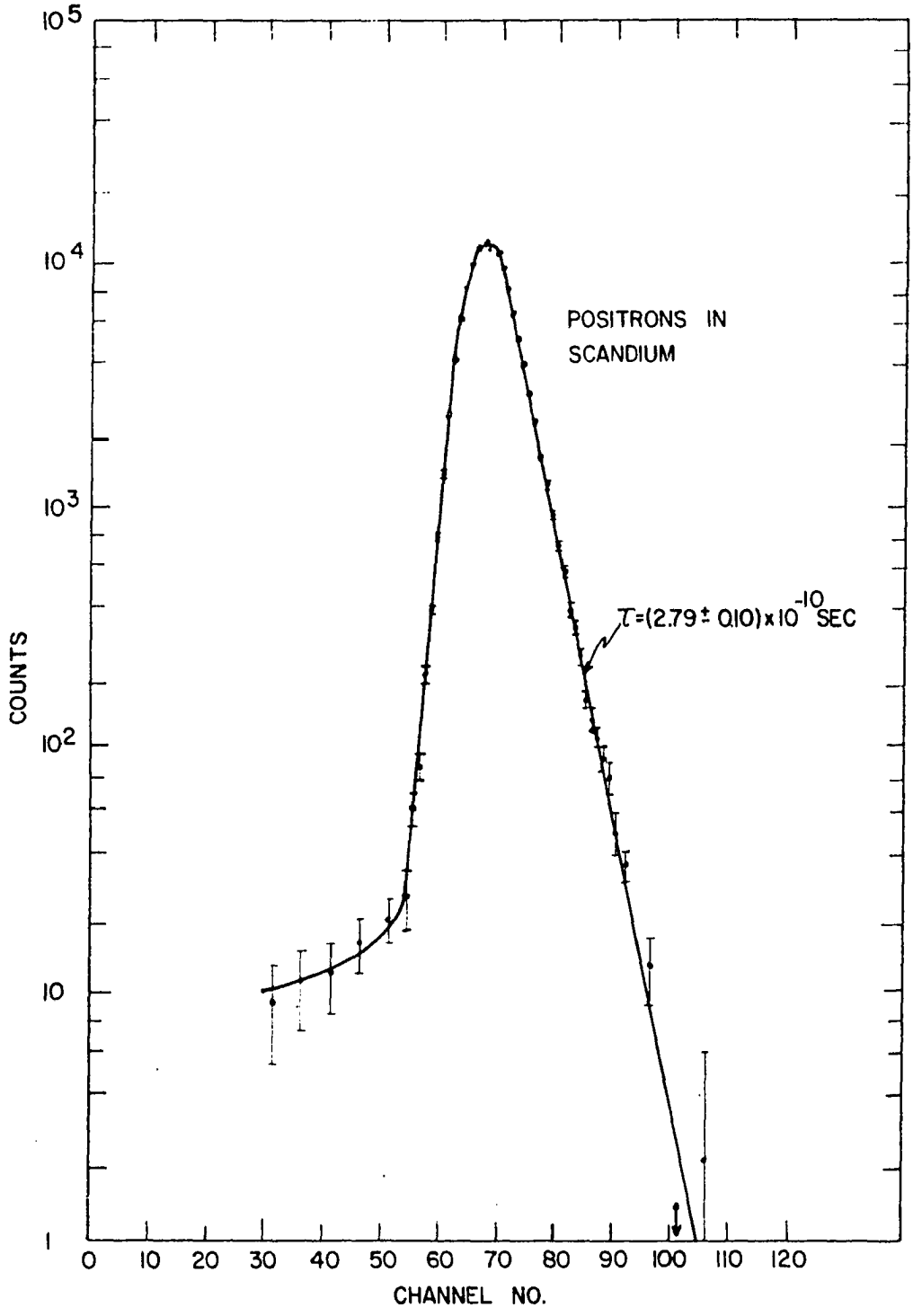
POSITRONS IN
SCANDIUM
τ=(2.79 ± 0.10)x10^-10 SEC
COUNTS
CHANNEL NO.
10^5
10^4
10^3
10^2
10
1
0
10
20
30
40
50
60
70
80
90
100
110
120

Figure 22. Time spectrum of positron annihilation in cerium. The positron mean life obtained from the centroid shift measurement is $(2.87 \pm 0.03) \times 10^{-10}$ sec, using a time calibration of 7.135×10^{-11} sec/channel.

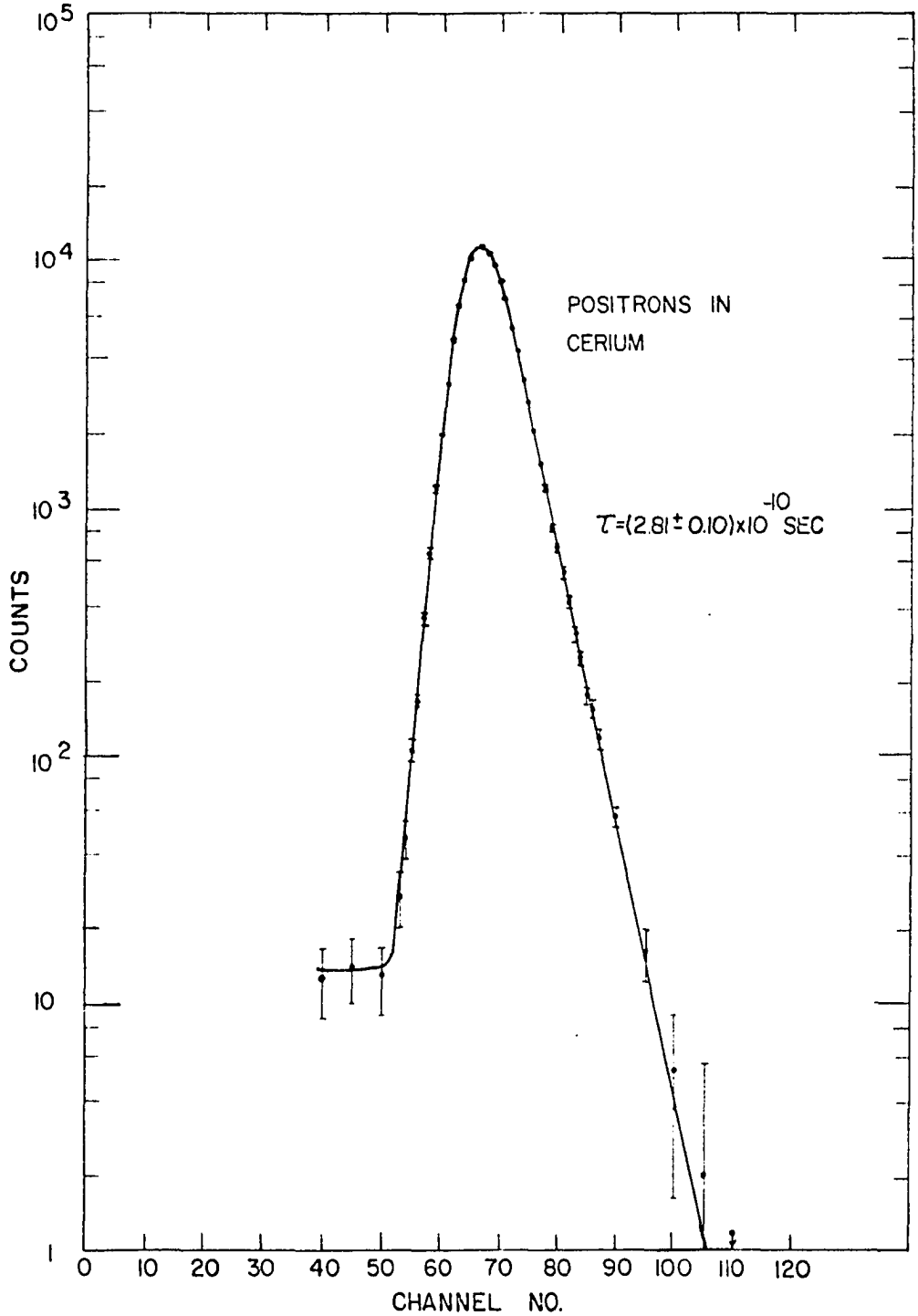
POSITRONS IN
CERIUM
τ=(2.81±0.10)x10^-10 SEC
COUNTS
CHANNEL NO.
10^5
10^4
10^3
10^2
10
1
0
10
20
30
40
50
60
70
80
90
100
110
120

Figure 23. Time spectrum of positron annihilation in europium. The positron mean life obtained from the centroid shift measurement is $(3.27 \pm 0.03) \times 10^{-10}$ sec, using a time calibration of 7.73×10^{-11} sec/channel.

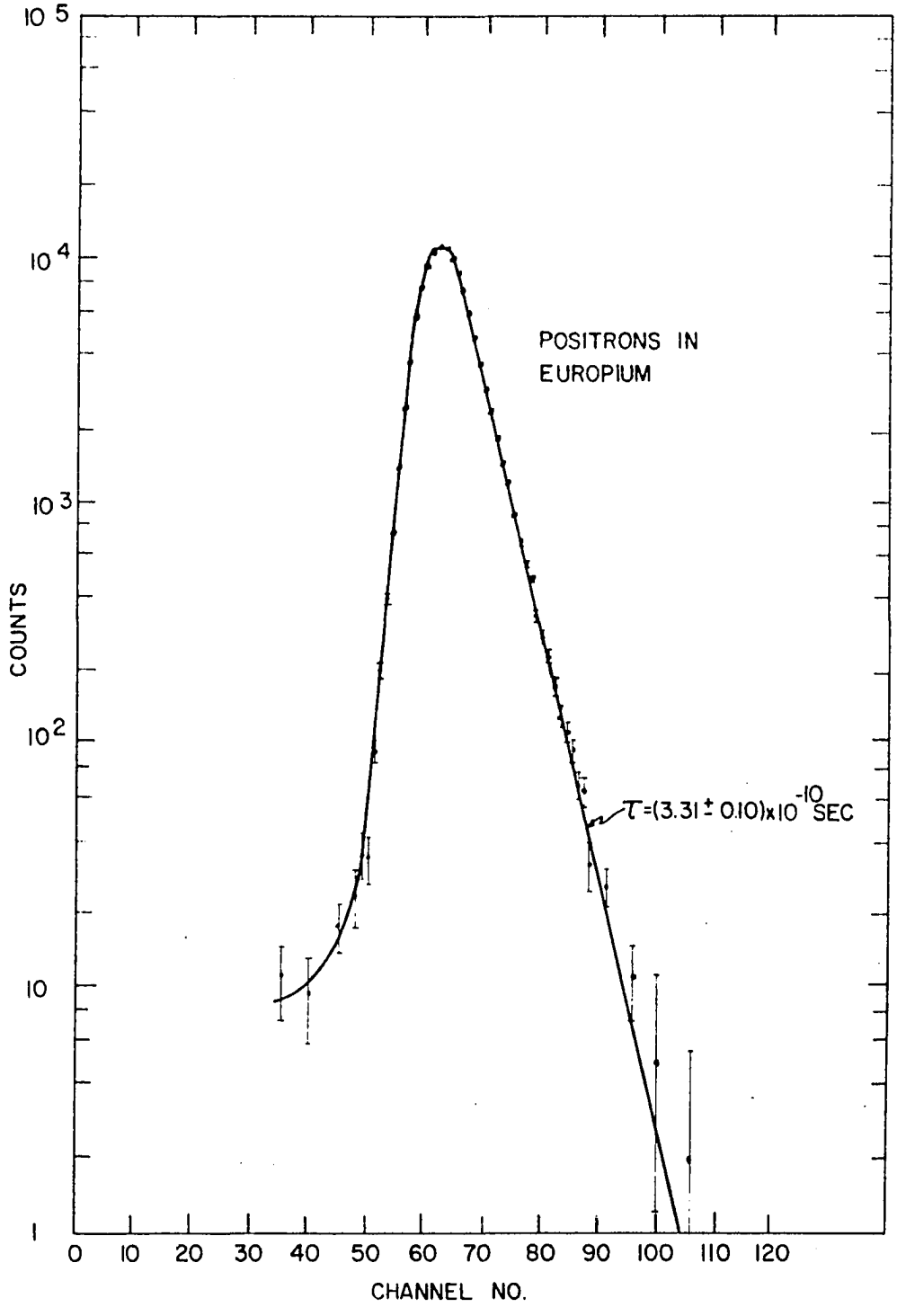
10 5
10 4
10 3
10 2
10
1
COUNTS
POSITRONS IN
EUROPIUM
τ=(3.31 ± 0.10)x10 -10 SEC
0 10 20 30 40 50 60 70 80 90 100 110 120
CHANNEL NO.

Figure 24. Time spectrum of positron annihilation in ytterbium. The positron mean life obtained from the centroid shift measurement is $(3.13 \pm 0.03) \times 10^{-10}$ sec, using a time calibration of 6.91×10^{-11} sec/channel.

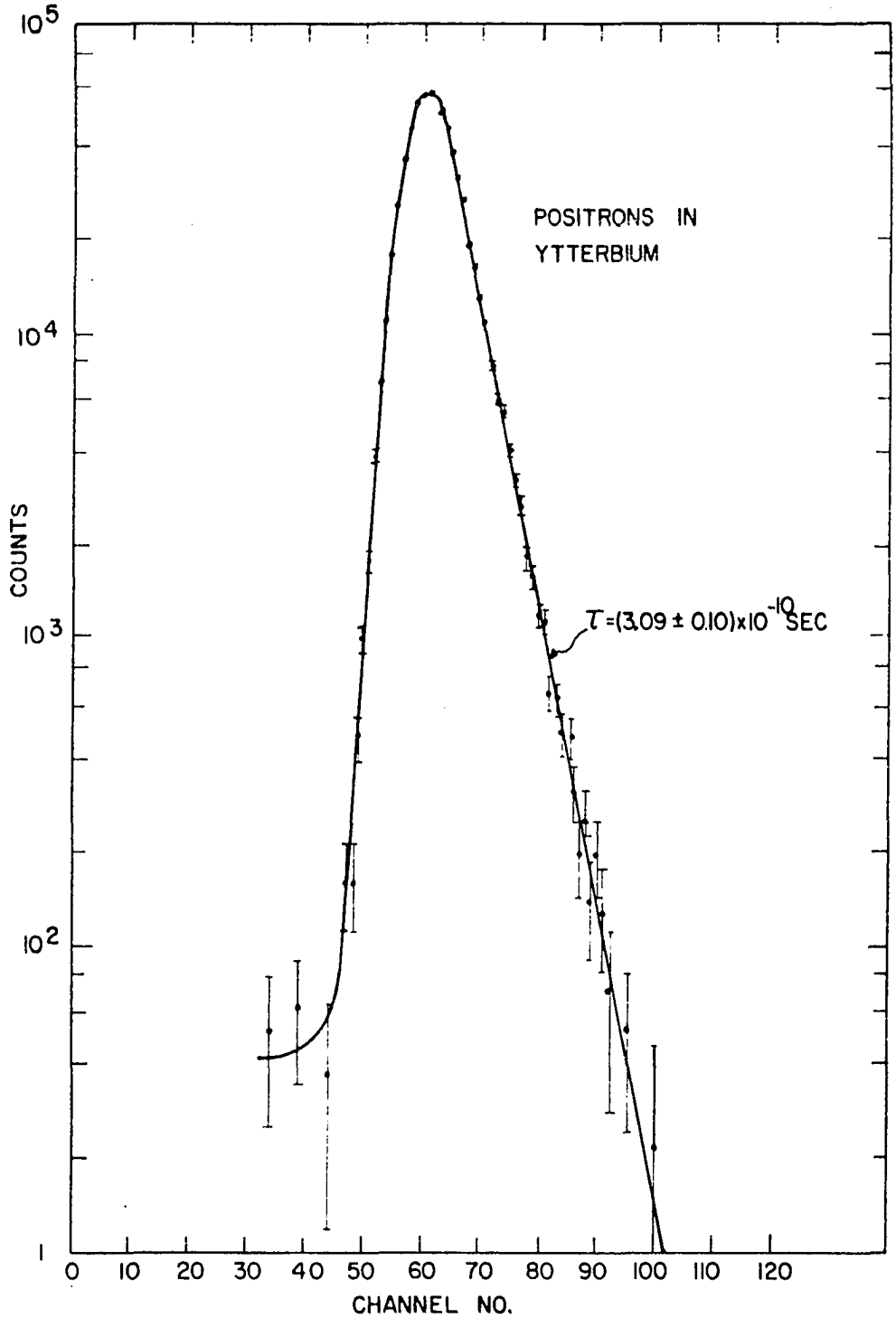
POSITRONS IN
YTTERBIUM
$\tau = (3.09 \pm 0.10) \times 10^{-10}$ SEC
COUNTS
CHANNEL NO.
10^5
10^4
10^3
10^2
1
0
10
20
30
40
50
60
70
80
90
100
110
120

Figure 25. Positron mean life versus x for Na_xWO_3. Several different methods were used to construct the source-sample sandwiches. The results obtained using the 0.25 mil aluminum foil source holders are believed to be the most reliable.

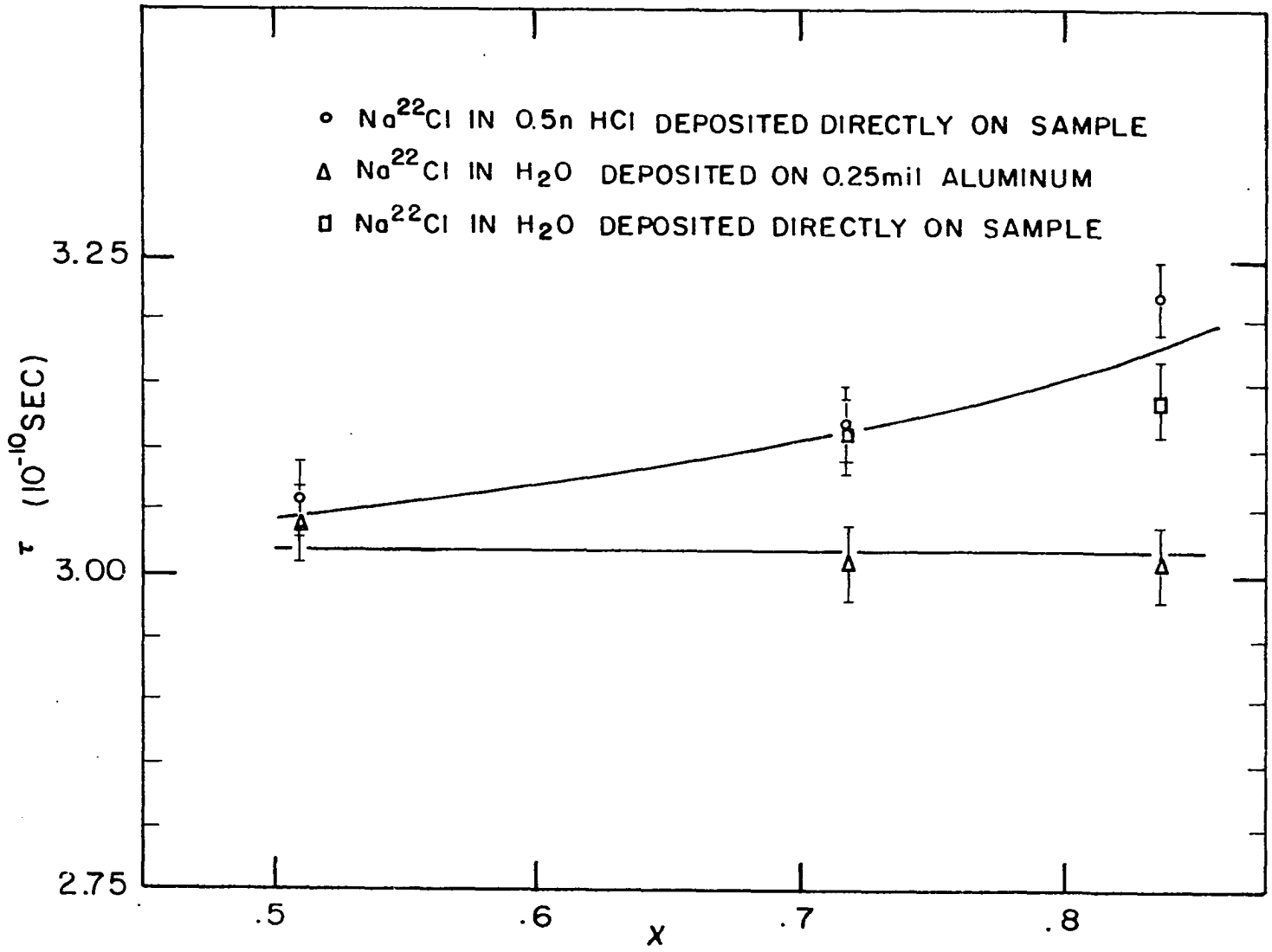
o $Na^{22}Cl$ IN 0.5n HCl DEPOSITED DIRECTLY ON SAMPLE
Δ $Na^{22}Cl$ IN H_2O DEPOSITED ON 0.25mil ALUMINUM
□ $Na^{22}Cl$ IN H_2O DEPOSITED DIRECTLY ON SAMPLE
3.25
3.00
2.75
τ (10^{-10}SEC)
.5
.6
.7
.8
X

the sodium, then one might expect the positron lifetime to decrease as x is increased. (The atomic volume is a very weak function of x.) Actually, however, the lifetime seems to increase with x as indicated by the upper curve in Figure 25. To see whether the acid solution used to make the positron sources might be responsible for the increase in lifetime with x, new samples were made for x = 0.717 and x = 0.835, this time using $Na^{22}Cl$ dissolved in distilled water. The new measurements (shown by the squares in Figure 25), however, yielded almost the same lifetimes as the previous measurements.

Finally, new samples were made for all three of the bronzes. The positron source (dissolved in distilled water) was deposited between two pieces of 0.25 mil aluminum foil, and then it was sandwiched between two pieces of Na_xWO_3. This time the positron lifetimes, as shown by the triangles in Figure 25, were found to be the same for all three values of x, and approximately the same as that originally found for x = 0.51.

The time spectra for x = 0.51 are shown for the aluminum foil source and for the directly deposited source in Figures 26 and 27, respectively. Figures 28 and 29 show the time spectra for x = 0.835 with the aluminum foil source and the directly deposited source, respectively. A comparison of Figures 26 and 27 shows that the log slopes for the two x = 0.51 samples are almost the same, and the lifetimes determined

Figure 26. Time spectrum of positron annihilation in $Na_{0.51}WO_3$. The positron source was deposited on 0.25 mil aluminum foil. The positron mean life obtained from the centroid shift measurement is $(3.04 \pm 0.03) \times 10^{-10}$ sec, using a time calibration of 7.63×10^{-11} sec/channel.

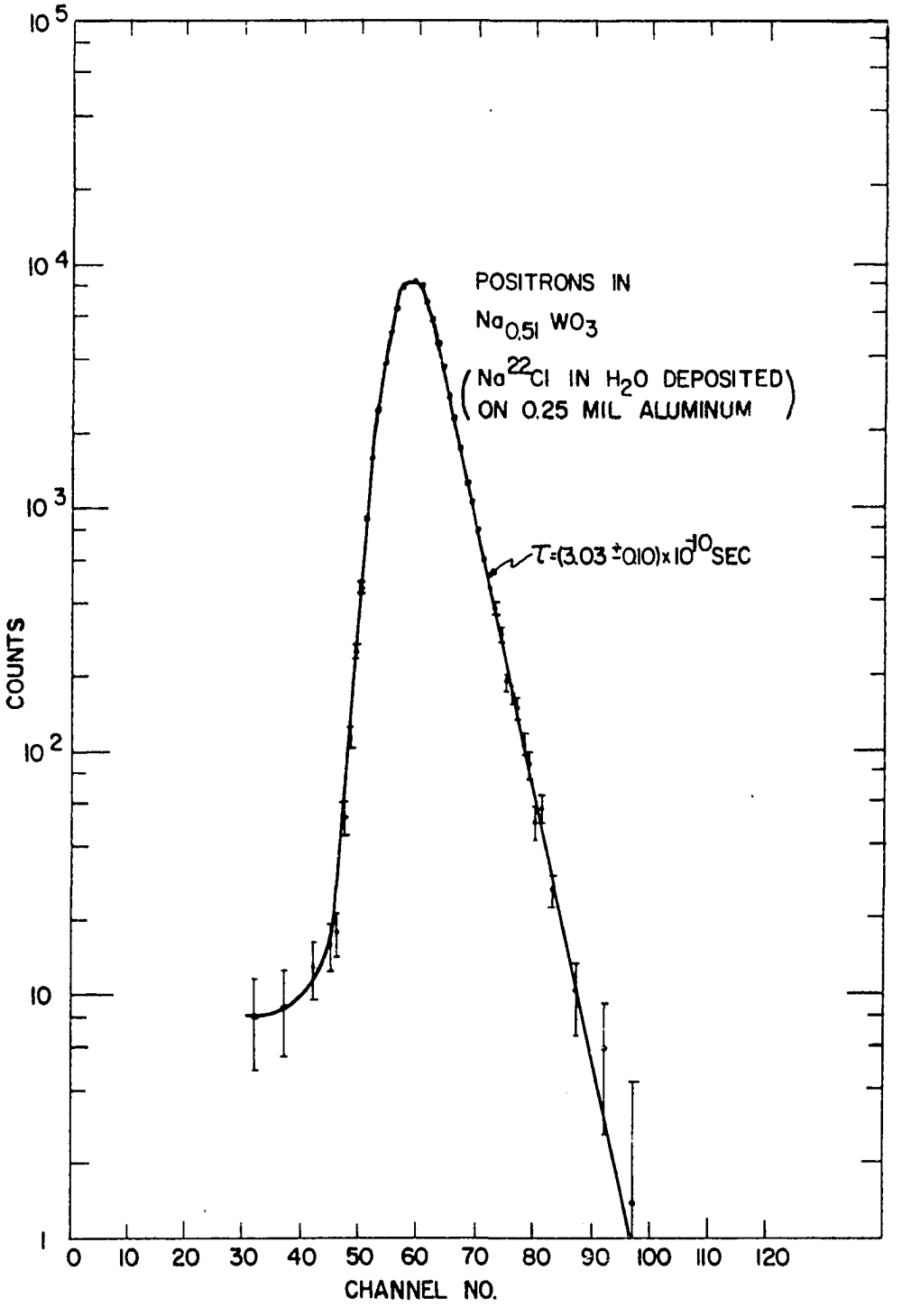
POSITRONS IN
$Na_{0.51}WO_3$
($Na^{22}Cl$ IN H_2O DEPOSITED ON 0.25 MIL. ALUMINUM)
$\tau=(3.03\pm0.10)\times10^{-10}$ SEC
COUNTS
CHANNEL NO.
10^5
10^4
10^3
10^2
10
1
0 10 20 30 40 50 60 70 80 90 100 110 120

Figure 27. Time spectrum of positron annihilation in $Na_{0.51}WO_3$. The positron source (dissolved in 0.5 normal HCl) was deposited directly on the sample. The time calibration is 5.39×10^{-11} sec/channel. The positron mean life obtained from a centroid shift measurement is $(3.06 \pm 0.03) \times 10^{-10}$ sec.

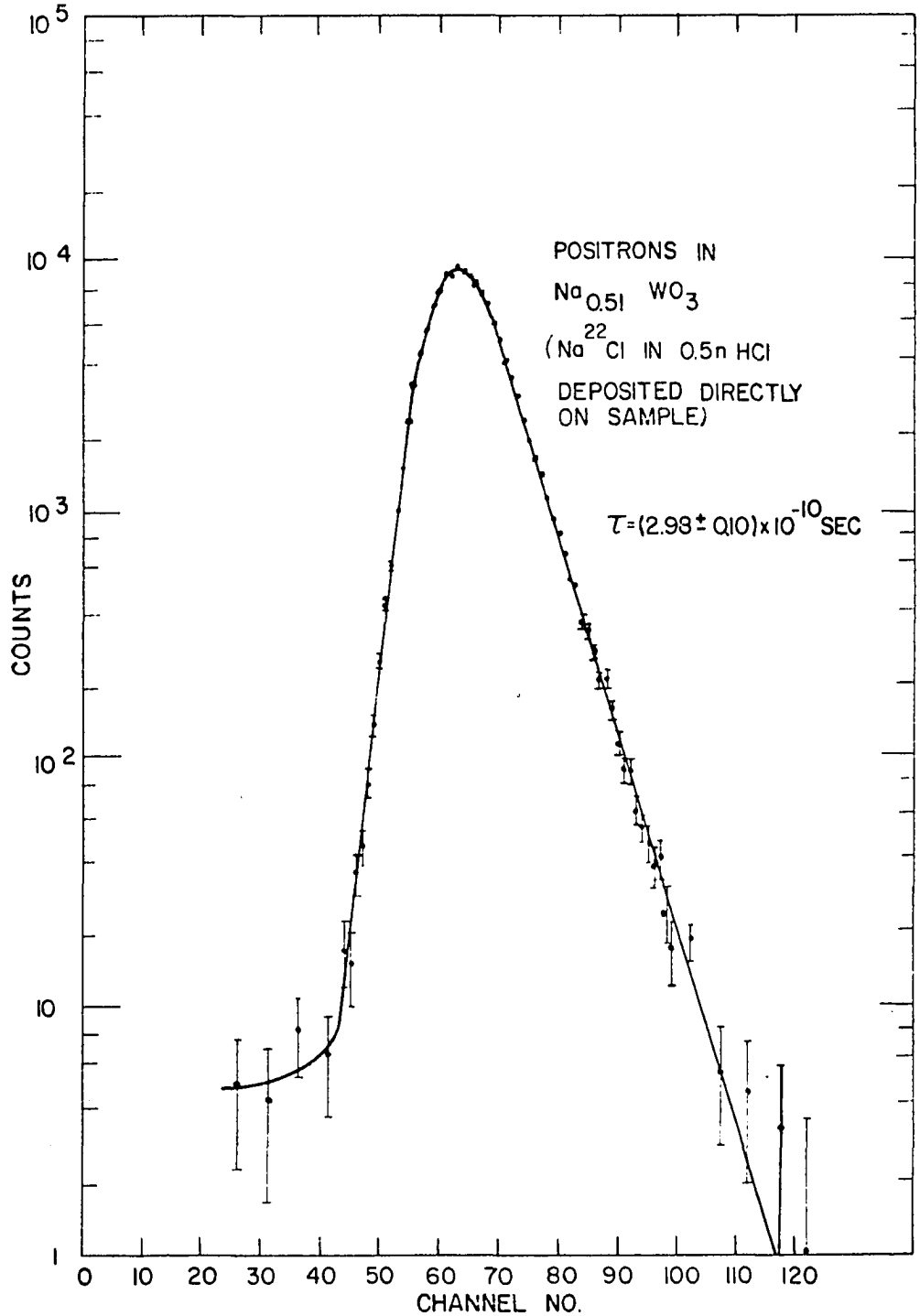
POSITRONS IN
$Na_{0.51}WO_3$
($Na^{22}Cl$ IN 0.5n HCl
DEPOSITED DIRECTLY
ON SAMPLE)
$\tau = (2.98 \pm 0.10) \times 10^{-10}$ SEC
COUNTS
CHANNEL NO.
10^5
10^4
10^3
10^2
10
1
0
10
20
30
40
50
60
70
80
90
100
110
120

Figure 28. Time spectrum of positron annihilation in $Na_{0.835}WO_3$. The positron source was deposited on 0.25 mil aluminum foil. The time calibration is 7.645×10^{-11} sec/channel. The positron mean life obtained from a centroid shift measurement is $(3.01 \pm 0.03) \times 10^{-10}$ sec.

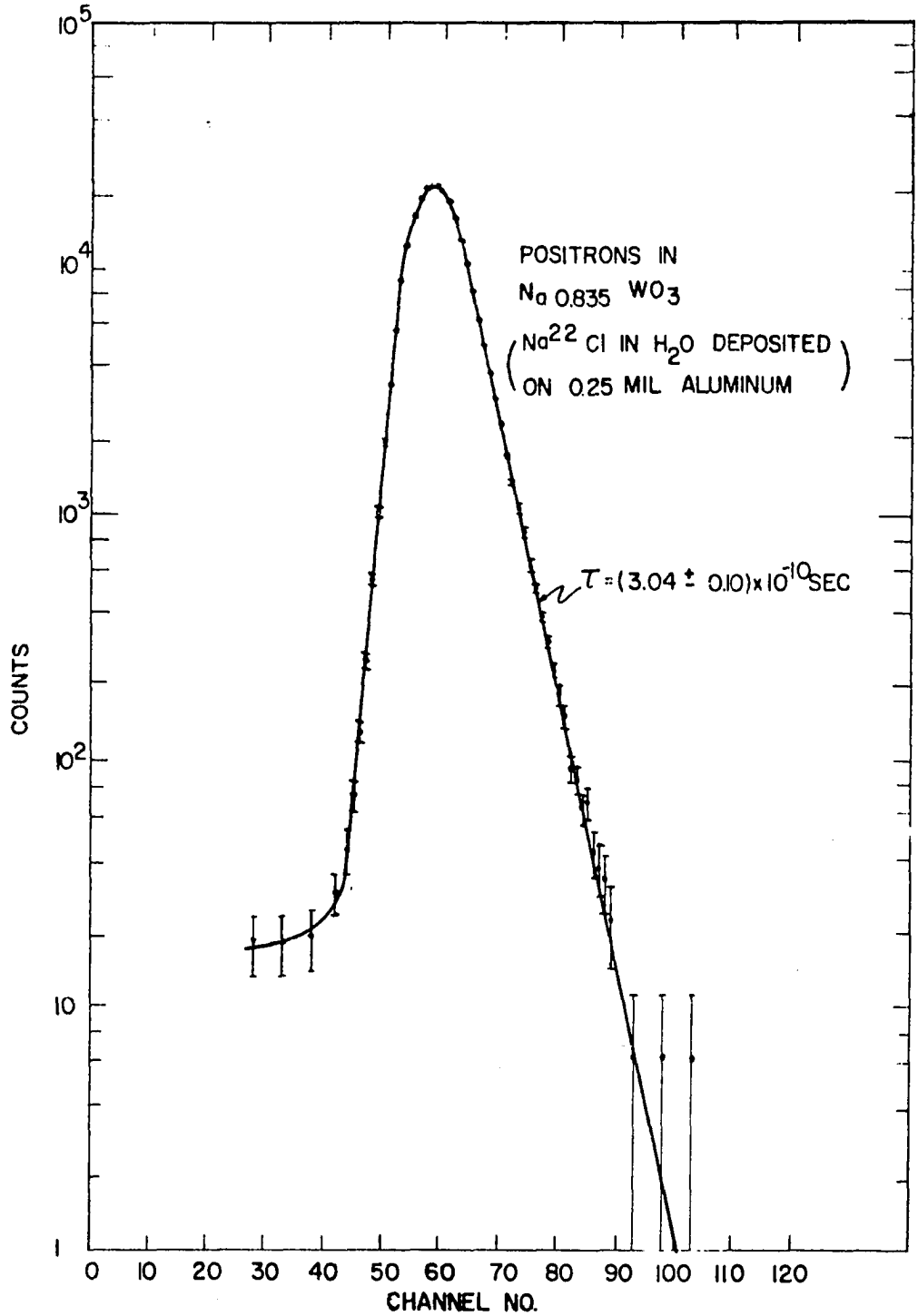
POSITRONS IN
Na 0.835 WO3
(Na22 Cl IN H2O DEPOSITED
ON 0.25 MIL ALUMINUM)
τ = (3.04 ± 0.10) x 10-10 SEC
COUNTS
CHANNEL NO.
10^5
10^4
10^3
10^2
10
1
0 10 20 30 40 50 60 70 80 90 100 110 120

Figure 29. Time spectrum of positron annihilation in $Na_{0.835}WO_3$. The positron source (dissolved in 0.5 normal HCl) was deposited directly on the sample. The time calibration is 7.645×10^{-11} sec/channel. The positron mean life obtained from a centroid shift measurement is $(3.22 \pm 0.03) \times 10^{-10}$ sec. Note the tail on the spectrum, indicating the presence of a long lifetime component.

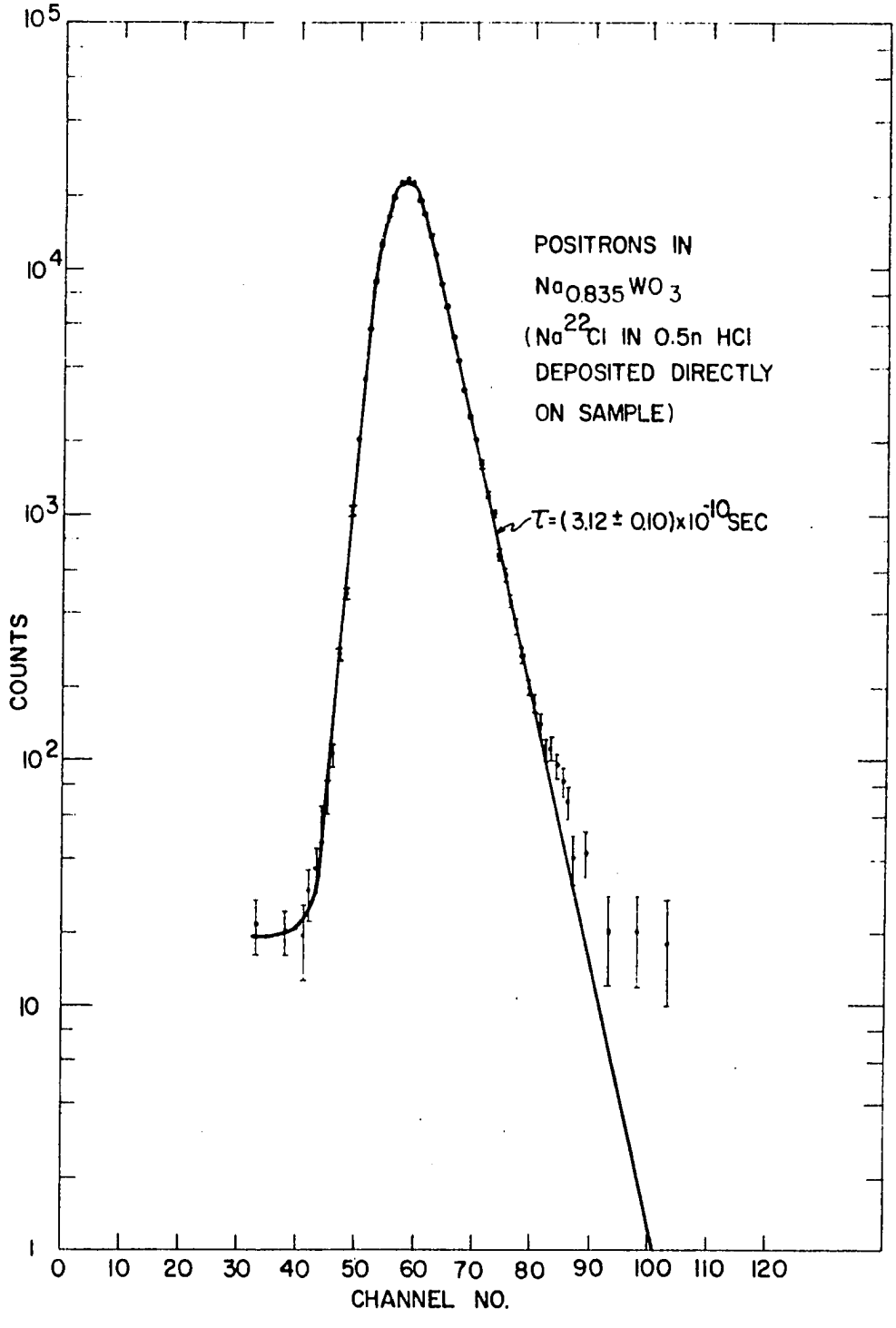
POSITRONS IN
$Na_{0.835}WO_3$
($Na^{22}Cl$ IN 0.5n HCl
DEPOSITED DIRECTLY
ON SAMPLE)
$\tau = (3.12 \pm 0.10) \times 10^{-10}$ SEC
COUNTS
CHANNEL NO.
10^5
10^4
10^3
10^2
10
1
0
10
20
30
40
50
60
70
80
90
100
110
120

from the slopes agree very well with the measured centroid shifts. Figure 29, however, has a tail which indicates the presence of a long lived component for the x = 0.835 sample which had the directly deposited source. This tail, on the other hand, is not present in the time spectrum for the x = 0.835 sample which had the aluminum foil source holder.

The data obtained using the aluminum foil source holders are thought to be the most reliable, for they can not be in error because of any surface effects. Also, as mentioned in connection with the rare earths, the errors due to positron annihilation in the aluminum should be quite small. Thus the positron lifetime probably remains constant as x is varied from 0.51 to 0.835. The greater centroid shift obtained for the larger x values when using a directly deposited source apparently is due to the appearance of a small percentage ($\sim$ 5-10%) of a long lived component ($\tau_2 \sim 3.5\text{-}6 \times 10^{-10}$ sec) in the lifetime. This τ_2 component seems to be due to some type of surface effect that is not important for x = 0.51, but becomes more serious as x is increased. None of the measurements indicate any decrease in the positron lifetime as x is increased, although this is what should occur if the sodium atoms furnish the conduction electrons with which the positrons annihilate.

The positron mean life was also measured for tungsten trioxide (WO_3). Powdered WO_3 was compressed into two

disks with a hydraulic press. The source was deposited between two pieces of 0.25 mil aluminum foil and then sandwiched between the two disks of WO_3. The lifetime measured by the centroid shift technique was $(3.40 \pm 0.03) \times 10^{-10}$ sec, while the log slope gave a lifetime of $(3.60 \pm 0.15) \times 10^{-10}$ sec. The time spectrum for WO_3 is shown in Figure 30.

Figure 30. Time spectrum of positron annihilation in WO_3. The positron mean life obtained from the centroid shift measurement is $(3.40 \pm 0.03) \times 10^{-10}$ sec, using a time calibration of 5.50×10^{-11} sec/channel.

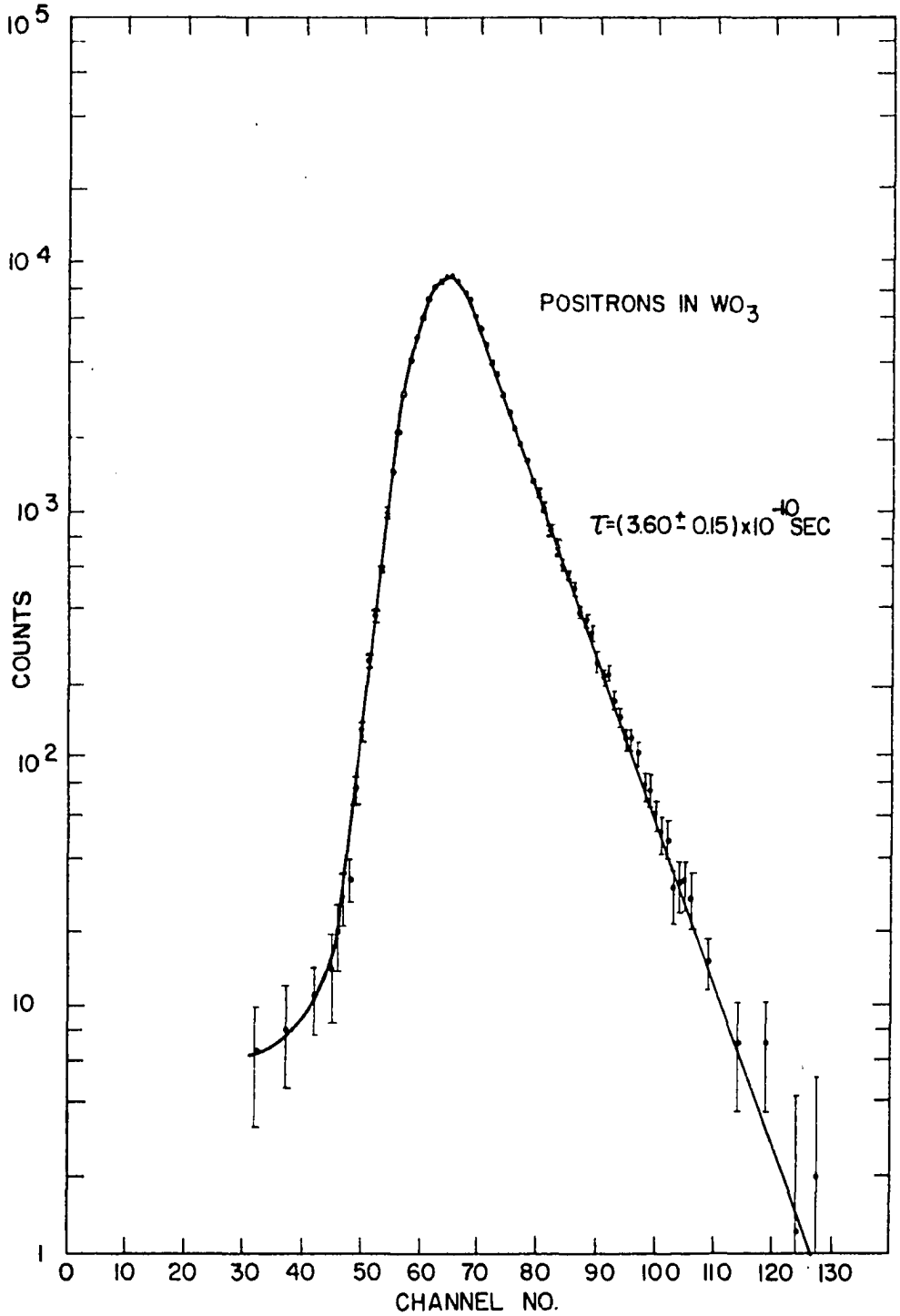
POSITRONS IN WO_3
$\tau=(3.60\pm0.15)\times10^{-10}$ SEC
COUNTS
CHANNEL NO.
10^5
10^4
10^3
10^2
10
1
0
10
20
30
40
50
60
70
80
90
100
110
120
130

V. SUMMARY AND CONCLUSIONS

The measurements of positron lifetimes in the sodium tungsten bronzes indicate that great care must be taken when making the source-sample sandwiches, in order to avoid complications due to possible surface effects. These measurements also indicate that a study of the log slopes of the time spectra supplements the centroid shift measurements in an important way, for such a study may reveal the presence of more than one characteristic lifetime. The apparent insensitivity of the positron lifetime to the sodium concentration in the sodium tungsten bronzes remains unexplained.

The present investigation has confirmed the presence of the τ_2 lifetime in aluminum as reported by Gerholm (50) and by Bell and Jørgensen (28). The reason for this long lived component, however, remains to be explained. The aluminum measurements have also shown the importance of using a compensation circuit when making absolute lifetime measurements with the centroid shift method.

The trivalent rare earth metals all have nearly the same r_s' value, and within statistics the measured positron lifetimes are also nearly the same for all of them. The two divalent rare earths have appreciably larger r_s' values, and the measured positron lifetimes are significantly larger for these metals. Scandium, however, has a smaller r_s' than the trivalent

rare earths, and the measured positron lifetime in scandium is correspondingly smaller. The measurements have also established the fact that the 4f electrons are indeed well shielded. Thus the positron should be a valuable tool for exploring the electronic structure of solids. Because of the strong influence of the positron on its surroundings, however, the variation of the annihilation rate with r_s' seems to be $\propto r_s'^{-1/2}$ rather than the much stronger $r_s'^{-3}$ dependence predicted by the free electron theory. For this reason very accurate measurements are necessary, and it has been shown that the centroid shift technique allows positron lifetimes to be measured with the accuracy required. The present theories on positron annihilation do not satisfactorily explain the experimental results, and a great deal of theoretical work remains to be done before detailed conclusions can be drawn from measurements of positron lifetimes.

The phenomenon of core annihilation complicates the interpretation of positron lifetime measurements. It has been shown, however, that certain elements can be grouped together because of their similar core configurations. Perhaps, then, a systematic exploration of the elements by positron lifetime measurements would yield families of elements which exhibit a smooth variation of the positron annihilation rate with r_s'. If this were to be the case, then the interpretation of the experimental results should be appreciably simplified.

VI. BIBLIOGRAPHY

1. Lee-Whiting, G. E. Thermalization of positrons in metals. Physical Review 97, 1557 (1955).

2. Ferrell, Richard A. Theory of positron annihilation in solids. Reviews of Modern Physics 28, 308 (1956).

3. Bell, R. E. and R. L. Graham. Complex time decay of positrons annihilated in condensed materials. Physical Review 87, 236 (1952).

4. _____ and _____. Time distribution of positron annihilation in liquids and solids. Physical Review 90, 644 (1953).

5. DeBenedetti, S., C. E. Cowan, W. R. Konneker, and H. Primakoff. On the angular distribution of two-photon annihilation radiation. Physical Review 77, 205 (1950).

6. Garwin, R. L. Thermalization of positrons in metals. Physical Review 91, 1571 (1953).

7. Yang, C. N. Selection rules for the dematerialization of a particle into two photons. Physical Review 77, 242 (1950).

8. Ore, A. and J. L. Powell. Three-photon annihilation of an electron-positron pair. Physical Review 75, 1696 (1949).

9. Deutsch, Martin. Annihilation of positrons. Progress in Nuclear Physics 3, 131 (1953).

10. DeBenedetti, S. and H. C. Corben. Positronium. Annual Review of Nuclear Science 4, 191 (1954).

11. DeBenedetti, S. Annihilation of positrons. In Siegbahn, Kai, ed. Beta- and gamma-ray spectroscopy. pp. 672-679. North-Holland Publishing Co., Amsterdam, The Netherlands. 1955.

12. Bell, R. E. Annihilation of positrons in liquids and solids. In Siegbahn, Kai, ed. Beta- and gamma-ray spectroscopy. pp. 680-688. North-Holland Publishing Co., Amsterdam, The Netherlands. 1955.

13. Berko, Stephan and Frank L. Hereford. Experimental studies of positron interactions in solids and liquids. Reviews of Modern Physics 28, 299 (1956).

14. Wallace, Philip R. Positron annihilation in solids and liquids. Solid State Physics 10, 1 (1960).

15. Rich, J. A. Experimental evidence for the three-photon annihilation of an electron-positron pair. Physical Review 81, 140 (1951).

16. Basson, J. K. Direct quantitative observation of the three-photon annihilation of a positron-negatron pair. Physical Review 96, 691 (1954).

17. Graham, R. L. and A. T. Stewart. Three-quantum annihilation of positrons in solids. Canadian Journal of Physics 32, 678 (1954).

18. Green, R. E. and A. T. Stewart. Angular correlation of photons from positron annihilation in light metals. Physical Review 98, 486 (1955).

19. Stewart, A. T. Angular correlation of photons from positron annihilation in solids. Physical Review 99, 594 (1955).

20. _____. Momentum distribution of metallic electrons by positron annihilation. Canadian Journal of Physics 35, 168 (1957).

21. Lang, G., S. DeBenedetti, and R. Smoluchowski. Measurement of electron momentum by positron annihilation. Physical Review 99, 596 (1955).

22. Lang, G. and S. DeBenedetti. Angular correlation of annihilation radiation in various substances. Physical Review 108, 914 (1957).

23. Berko, Stephan and John S. Plaskett. Correlation of annihilation radiation in oriented single metal crystals. Physical Review 112, 1877 (1958).

24. Stewart, A. T., J. B. Shand, J. J. Donaghy, and J. H. Kusmiss. Fermi surface of beryllium by positron annihilation. Physical Review 128, 118 (1962).

25. Berko, Stephan. Band structure and positron annihilation in metals: Be and Mg. [To be published in Physical Review ca. 1963].

26. Page, L. A., M. Heinberg, J. Wallace, and T. Trout. Angular correlation in two-photon annihilation in quartz. Physical Review 98, 206 (1955).

27. Dirac, P. A. M. On the annihilation of electrons and protons. Proceedings of the Cambridge Philosophical Society 26, 361 (1930).

28. Bell, R. E. and M. H. Jørgensen. Mean lives of positrons in aluminum and the alkali metals. Canadian Journal of Physics 38, 652 (1960).

29. Bisi, A., G. Faini, E. Gatti, and L. Zappa. Positron lifetime in metals. Physical Review Letters 5, 59 (1960).

30. Jones, G. and J. B. Warren. The lifetimes of positrons in metals. Canadian Journal of Physics 39, 1517 (1961).

31. Schiff, Leonard I. Quantum mechanics. 2nd ed. New York, N. Y., McGraw-Hill Book Co., Inc. 1955.

32. Bohm, David and David Pines. A collective description of electron interactions. III. Coulomb interactions in a degenerate electron gas. Physical Review 92, 609 (1953).

33. Kahana, S. Positron annihilation in metals. Physical Review 117, 123 (1960).

34. Bethe, H. A. and J. Goldstone. Effect of a repulsive core in the theory of complex nuclei. Proceedings of the Royal Society (London) Series A, 238, 551 (1957).

35. Fairstein, Edward and F. M. Porter. A fast differential pulse-height selector circuit. Review of Scientific Instruments 23, 650 (1952).

36. Fairstein, Edward. Improved differential pulse-height selector circuit. Review of Scientific Instruments 27, 549 (1956).

37. Simms, P. C. Fast coincidence system based on a transistorized time-to-amplitude converter. Review of Scientific Instruments 32, 894 (1961).

38. Garwin, R. L. A useful fast coincidence circuit. Review of Scientific Instruments 21, 569 (1950).

39. Madey, Richard. Fast counting system for high-energy particle measurements. Review of Scientific Instruments 26, 971 (1955).

40. Bell, R. E., R. L. Graham, and H. E. Petch. Design and use of a coincidence circuit of short resolving time. Canadian Journal of Physics 30, 35 (1952).

41. Ippolito, Fred. Transistor controls temperature. Popular Electronics 16, No. 4, 46 (April 1962).

42. Lundby, Arne. Scintillation decay times. Physical Review 80, 477 (1950).

43. Post, R. F. and L. I. Schiff. Statistical limitations on the resolving time of a scintillation counter. Physical Review 80, 1113 (1950).

44. Birks, J. B. Scintillation counters. New York, N. Y., McGraw-Hill Book Co., Inc. 1953.

45. Newton, T. D. Decay constants from coincidence experiments. Physical Review 78, 490 (1950).

46. Bay, Z. Calculation of decay times from coincidence experiments. Physical Review 77, 419 (1950).

47. Simms, P. C., N. Benczer-Koller, and C. S. Wu. New application of delayed coincidence techniques for measuring lifetimes of excited nuclear states-- Ca^{42} and Sc^{47}. Physical Review 121, 1169 (1961).

48. Chaplin, G. B. B. and C. J. N. Candy. A transistor circuit for fast coincidence measurements. Nuclear Instruments and Methods 5, 242 (1959).

49. Jones, G. Experimental lifetimes of positrons in metals. Bulletin of the American Physical Society Series 2, 4, 367 (1959).

50. Gerholm, T. R. On the annihilation of positrons in condensed materials. Arkiv för Fysik 10, 523 (1956).

VII. ACKNOWLEDGMENTS

The author gratefully acknowledges the contributions of the following people to the successful completion of the present investigation:

Dr. M. G. Stewart, who suggested the problem and whose continuing aid and encouragement were invaluable.

Mr. J. E. Griffin, who designed the time-amplitude converter and offered many helpful suggestions on the design and operation of other electronic circuits.

Mr. G. E. Holland, who helped to keep the multichannel analyzer in satisfactory working condition.

Mr. W. W. Souder, who helped with the centroid shift computations and the plotting of data.

Dr. A. H. Daane's group of the Ames Laboratory of the U. S. Atomic Energy Commission, who furnished the rare earth samples.

Dr. G. C. Danielson's group of the Ames Laboratory of the U. S. Atomic Energy Commission, who furnished the sodium tungsten bronze samples.